PNPT1-mtRNA axis mediates chemotherapy-induced immune signaling and can be targeted to overcome therapeutic resistance

Mingfu Tian[1#], Siyu Liu[1#], Xu Li[1#], Zelin Chai[1], Zhiqiang Li[1], Hong Fan[2], Chengliang Zhu**[2], Kailang Wu[1]**, Ke Lan[1,3,4,5]*

[1]State Key Laboratory of Virology and Biosafety, College of Life Sciences, Wuhan University, Wuhan 430072, China.

[2]Department of Clinical Laboratory, Renmin Hospital, Wuhan University, Wuhan 430060, China.

[3]Department of Infectious Diseases, Frontier Science Center for Immunology and Metabolism, Medical Research Institute, Zhongnan Hospital of Wuhan University, Wuhan University, Wuhan 430071, China.

[4]Taikang Center for Life and Medical Sciences, Wuhan University, Wuhan 430071, China.

[#]These authors contributed equally to this work.

[5]Lead contact: Ke Lan, E-mail: klan@whu.edu.cn

****Co-corresponding authors**. Kailang Wu, Chengliang Zhu

Abstract

Immunity against malignant cells and the ability of cancer cells to escape anticancer immunity constitute the core process of tumor development, but the underlying mechanism is still largely unknown. Through integrated analyses of clinical samples, cellular assays, and multiple murine tumor models, our study provides compelling evidence that mitochondrial RNA (mtRNA)-derived danger signals potently activate antitumor immunity and uncovers a tumor-specific mechanism for dampening mtRNA-mediated immune responses. Mechanistically, antitumor therapies facilitate the release of immunogenic mitochondrial double-stranded RNA, which potently activates the MAVS signaling cascade and elicits robust antitumor immune responses. Notably, the pan-tumoral expression of MAVS and its upstream receptors enables broad-spectrum mtRNA-driven immune activation across diverse cancer types. In contrast, malignant cells and tumor microenvironments upregulate PNPT1 to degrade immunogenic mitochondrial RNA structures, forming a negative feedback loop that subverts immune surveillance. Importantly, pharmacological inhibition of PNPT1 synergizes with BH3-mimetic drugs to potently amplify mtRNA-mediated antitumor immunity, overcoming therapeutic resistance without apparent systemic toxicity. Our findings suggest that inducing mtRNA-related danger signals in combination with PNPT1 inhibition holds promise as an innovative strategy for anticancer therapy.

Keywords:

chemotherapy; antitumor immunity; mt dsRNA; MAVS; PNPT1; cancer immunotherapy

Introduction

Our bodies are perpetually challenged by external menaces like viral/bacterial infections, as well as internal threats such as malignant cell transformation and oncogenesis. A prompt defense against these insults is vital for maintaining homeostasis[1-3]. Host cells deploy an arsenal of innate immune signaling cascades to detect both exogenous and endogenous danger cues, triggering immune effectors for pathogen/tumor clearance[4]. Pathogen-associated molecular patterns (PAMPs) released by microbes efficiently engage pattern recognition receptors on host cells, igniting innate immunity[1,5]. Intriguingly, antitumor modalities like chemotherapy and radiotherapy also harness innate immune mechanisms to bolster immunosurveillance[6,7], but the underlying activation mechanisms remain incompletely understood.

Chemotherapy plays a pivotal role in the clinical management of malignant tumors. Accumulating evidence from previous studies has demonstrated that beyond its direct cytotoxic effect of eliminating tumor cells, chemotherapy can also elicit robust immunogenic responses that contribute to tumor regression[6,8,9]. Specifically, the immunogenic responses induced by chemotherapy are multifaceted, encompassing two distinct yet interconnected mechanisms. On one hand, it directly potentiates the activity of the innate immune system by upregulating the expression of pattern recognition receptors, pro-inflammatory cytokines, and other immune-modulatory molecules in immune cells. On the other hand, it exerts a secondary effect triggered by the release of damage-associated molecular patterns (DAMPs) and tumor-associated antigens (TAAs) from dying tumor cells. These danger signals alert the host immune system to the presence of neoplastic cells, thereby initiating a cascade of adaptive immune responses characterized by the activation and proliferation of tumor-reactive T lymphocytes, which further reinforce the anti-tumor efficacy of chemotherapy[7,9,10]. Type I IFNs are primarily produced by cells that activate innate immune responses[6]. Previously, anti-tumor innate

immunotherapies mainly targeted the cGAS-STING pathway[11,12]. However, decreased STING levels in cancer tissue consistently led to poor treatment outcomes when targeting STING. Nonetheless, chemotherapies that activate innate immunity can still yield positive results in tumors with low STING levels, indicating the existence of broader innate immunity activation pathways that do not rely on STING[13-19].

Our study uncovers a pivotal role for mitochondrial RNA (mtRNA)-derived danger signals in activating innate immunity during antitumor therapy. Chemotherapy elicits a robust immunostimulatory response by inducing the release of immunogenic mitochondrial double-stranded RNA (mt-dsRNA), a process that potently activates immune surveillance mechanisms. Mechanistically, this therapeutic modality promotes the translocation of mt-dsRNA into the cytoplasm through BAK/BAX-dependent pore formation, thereby amplifying antitumor immunity. Notably, the danger signals emanating from mtRNA engage the RIG-I/MDA5-MAVS signaling axis—a pathway ubiquitously expressed in tumor tissues. This ensures broad-spectrum activation of antitumor immune responses, effectively circumventing tumor-mediated immune evasion strategies.

Malignant cells employ sophisticated strategies to evade immune detection[20-22]. Our data reveal that malignant cells upregulate PNPT1, an enzyme that degrades immunogenic mitochondrial nucleic acids, thereby dampening immune activation and evading immunosurveillance. Clinical analyses confirm that PNPT1 overexpression in tumor tissues correlates with immune escape and disease progression. Critically, PNPT1 knockdown potentiates anticancer immunity, synergizing with chemotherapy and PD-1 immunotherapy. Targeting the mtRNA-MAVS axis represents an unexploited therapeutic frontier. Addressing this unmet need, we have developed therapeutic strategy targeting the PNPT1-mtRNA axis. Combinatorial therapy using an FDA-approved PNPT1 inhibitor and BH3-mimetic agents reactivates antitumor immunity, overcomes solid tumor resistance, and demonstrates favorable

92 safety profiles in preclinical models. These findings highlight its translational potential as a
93 safe and efficacious strategy to enhance cancer immunotherapy.
94
95
96 **Results**
97 **The Mavs pathway efficiently and broadly mediates chemotherapy-dependent immune**
98 **responses.**
99 Chemotherapy is the primary method for cancer treatment to kill malignant cells directly[23].
100 Previous studies have shown that chemotherapies activate the innate immune pathway to
101 enhance the anti-tumor immune response, with STING serving as the key regulator of this
102 process by binding to DNA released from the nucleus or mitochondria. However, emerging
103 evidence indicates that STING levels are decreased in various cancer types compared to normal
104 tissues, and the targets of STING have failed to activate innate immunity in cancer cells[13,14,19].
105 The enrichment analysis shows that chemotherapy still induce innate immune responses
106 in patient samples with lower STING expression in TCGA LIHC and LUAD datasets (Fig. 1a-
107 b), while the GEO datasets demonstrated that cisplatin (CIPT) treatment elicits type I interferon
108 and inflammatory responses in low-STING cell lines (Fig. 1c and S1b). Using the genotoxic
109 agent doxorubicin (DOX) and CIPT (both are commonly used chemotherapy drugs), we found
110 that both drugs induced IFN-β mRNA expression in medium-STING-expressing human
111 cervical cancer (HeLa) cells (Fig. S1c), low-STING-expressing lung (A549) and liver (HepG2)
112 cancer cells (Fig. S1d), and murine melanoma (B16) cells (Fig. S1e). DOX-mediated immune
113 responses were only partially reduced in STING-knockout human keratinocytes (HaCaT),
114 whereas the STING agonist cGAMP failed to induce responses (Fig. S1f), confirming that
115 chemotherapy triggers innate immunity independent of STING expression. These findings
116 suggest that DNA-mediated cGAS-STING activation is not the universal pathway for

chemotherapy-induced antitumor immunity, implying broader intracellular pathways exist.

Given the critical role of endogenous nucleic acids in activating immune responses[2], we analyzed all reported nucleic acid receptors and interferon-inducing pathways. Strikingly, the MAVS signaling axis and its upstream receptors RIG-I/MDA5 showed broader and higher expression in cancer cells compared to other receptors (Fig. S1g-h). Unlike STING, which is significantly reduced in multiple types of cancer validated by HPA-based IHC of lung cancer samples (Fig. 1e-f, S1a) [24], the RNA-responsive core protein MAVS (also known as VISA) [25,26] is either normally expressed or upregulated in tumors (Fig. 1d, S1i), which is validated by strong MAVS expression in lung cancer via HPA IHC slides (Fig. 1i). HPA data further show MAVS expression exceeds that of STING in multiple cancer types (Fig. 1h), suggesting a broader role for MAVS in mediating antitumor immunity.

Functional studies in HeLa cells transfected with siRNA targeting MAVS or STING (Fig. S1j-k) revealed that interfering with either partially inhibited chemotherapy-induced immune responses (Fig. 1i). In STING-knockout cells, chemotherapy still induced immune responses, which were abrogated by MAVS interference (Fig. 1j). In low-STING cancer cells, MAVS depletion alone suppressed chemotherapy-mediated immunity (Fig. 1k-l, S1k). The above results suggest that MAVS can efficiently mediate chemotherapy-induced immune responses regardless of STING expression. Specifically, in cancers with concurrent STING and MAVS expression, both molecules contribute to the immune response, whereas in STING-negative cancers, MAVS serves as the primary mediator. Additionally, DOX was found to enhance IFN-β mRNA expression in the mouse tumor cell line B16, which was abrogated following MAVS interference (Fig. 1m and S1k). Collectively, our findings demonstrate that the MAVS signaling pathway promotes immune responses during chemotherapy. Notably, the widespread expression of MAVS and its upstream RNA receptors in most cancer cells and tumor tissues allows these signals to initiate broad-spectrum antitumor immunity, thereby countering tumor

immune evasion mechanisms

Mitochondrial double-stranded RNA release triggers MAVS-dependent immune response.

Our findings demonstrate that MAVS can initiate an immune response. Previous studies have shown that MAVS and its upstream receptors primarily mediate RNA-dependent immune responses, encompassing both exogenous pathogenic microorganism infections and the host's own RNA [27]. As our system lacks exogenous infections, we focused on identifying which endogenous signals trigger the MAVS pathway. Host-derived RNA primarily originates from mitochondria and the nucleus. We first isolated mitochondrial and non-mitochondrial components from cells, purified their respective RNA, and transfected them into naïve cells to assess the immune-inducing capacity of RNA from different sources. The result shows that transfection of a low dose of mtRNA into recipient cells was sufficient to elicit robust immune responses. In striking contrast, even a tenfold higher dose of non-mitochondrial RNA failed to induce detectable immune activation. By integrating this observation into the context of our study, we further emphasized the critical role of mtRNA in mediating anti-tumor immunity, highlighting its potential as a key regulator in triggering tumor-reactive immune responses (Fig. 2a). Additionally, mtRNA from human tumor cells and primary mouse cells potently activated immune responses, indicating that the immunogenicity of mtRNA is an inherent property, unaffected by species or cellular background (Fig. S2a).

Given that RNA receptors reside in the cytoplasm, we next evaluated whether antitumor therapy induces mtRNA release into the cytoplasm. We separated cytoplasmic components and other cellular precipitates (mitochondria and other insoluble materials) (Fig. S2b), extracted cytoplasmic RNA, and quantified mtRNA content. Notably, mtRNAs such as cytochrome oxidase subunit 1 (Cox1) and cytochrome B (CytB) were significantly elevated in cytoplasmic

extracts from chemotherapeutic drug-treated HeLa cells (Fig. 2b). Similar results were observed in HepG2 and B16 cells, where chemotherapy promoted Cox1 mtRNA release into the cytoplasm (Fig. S2c, d). Collectively, these findings indicate that chemotherapy facilitates mtRNA release into the cytoplasm.

To investigate the role of cytoplasmic mtRNA in regulating immune responses, we isolated cytoplasmic RNAs (cRNAs) from CIPT-treated (cRNA-CIPT) or untreated (cRNA-Ctrl) donor HeLa and transfected them into recipient HeLa. IFN-β levels remained unchanged in recipient cells transfected with cRNA-Ctrl but were significantly enhanced by cRNA-CIPT (Fig. 2c), suggesting that cytoplasmic mtRNA release contributes to immune response induction. Subsequently, since mtRNA transcription is mediated by mitochondrial RNA polymerase (POLRMT)[28], we treated cells with the POLRMT inhibitor IMT1[29]. Chemotherapy-induced Cox1 mtRNA release into the cytoplasm was significantly inhibited in IMT1-treated cells (Fig. 2d), paralleled by a reduction in chemotherapy-induced immune responses (Fig. 2e). Transfecting recipient HeLa with cRNAs from CIPT-treated cells (cRNA) or CIPT plus IMT1-treated cells (cRNA-IMT1) further showed that IFN-β induction by cRNA was abrogated by IMT1 (Fig. 2f). The above results demonstrate that chemotherapeutic agents efficiently induce the release of mitochondrial RNA (mtRNA) into the cytoplasm, thereby activating immune responses.

To confirm MAVS dependency, we transfected mtRNA from B16 cells into wild-type (WT) and MAVS-knockout (MAVS-/-) MEFs. mtRNA induced IFN-β in WT MEFs but not in MAVS-/- MEFs (Fig. S2e), establishing MAVS as crucial for mtRNA-triggered immune responses during antitumor therapy. These results collectively demonstrate that chemotherapy promotes mtRNA release into the cytoplasm, driving MAVS-dependent immune activation. Previous studies indicate that intracellular RNA receptors like TLR3, MDA5, and RIG-I recognize specific RNA structures typically generated during viral infections[27,30]. We

hypothesized that mtRNA forms similar immunostimulatory structures. Using a monoclonal antibody (J2) to detect double-stranded RNA (dsRNA)[31], we observed dsRNA in normal uninfected cells, though less abundant than in vesicular stomatitis virus (VSV)-infected positive controls (Fig. 2g). Subcellular fractionation and J2 immunoprecipitation confirmed that mt-dsRNA localizes to mitochondria in untreated HeLa cells, not the cytoplasm (Fig. 2h), indicating basal mt-dsRNA presence in mitochondria. To test whether mtRNA immunogenicity relies on its double-stranded structure, we transfected mtRNA with or without dsRNA-specific RNase III treatment. Untreated mtRNA induced IFN-β mRNA in HeLa and MEF cells, while RNase III-treated mtRNA did not (Fig. 2i), confirming that dsRNA is essential for IFN-β induction. Under normal conditions, immunogenic nucleic acids are sequestered in mitochondria, separated from cytoplasmic receptors. Confocal microscopy showed that mt-dsRNAs localize to mitochondria under basal conditions but are released into the cytoplasm following CIPT or H2O2 treatment (Fig. 2j, k). RNA immunoprecipitation (RIP) validated that CIPT induces release of Cox1 and CytB mt-dsRNA into the cytoplasm of HeLa cells (Fig. 2l). Transfecting recipient cells with J2-purified dsRNA from chemotherapy-treated HeLa cytoplasm, but not J2-depleted RNA, significantly induced interferon, confirming that chemotherapy releases mitochondrial dsRNA into the cytoplasm to trigger immune responses.

Finally, we explored the mechanism of chemotherapy-induced mt-dsRNA release. Damaged cells often activate BAK/BAX pores, which facilitate mtDNA release, while mitochondrial permeability transition pores (mPTPs) and ANT2 pores may also play roles[32,33]. However, mPTP inhibition by Cyclosporin A (CSA) did not block Nd1/CytB mtRNA release in DOX-treated HeLa cells or Cox1/CytB/Nd5 release in CIPT-treated cells, nor did it affect post-chemotherapy immune responses (Fig. S3a-c). ANT2 interference similarly did not impact chemotherapy-induced mtRNA release (Fig. 2n, S3d), ruling out mPTPs and ANT2 in mt-dsRNA release. Conversely, the BAX inhibitor peptide V5 (BIP-V5) blocked CIPT-induced

Cox1/CytB mtRNA release (Fig. S3e) and IFN-β induction (Fig. S3f), while BAX knockdown inhibited mtRNA release and subsequent immune responses (Fig. 2o, p, S3g). These data establish that BAK/BAX pores are essential for mtRNA release and immune activation during chemotherapy. In conclusion, our study reveals that chemotherapy stimulates mitochondrial dsRNA release through BAK/BAX pores, triggering a MAVS-dependent immune response that combats tumor cells.

Tumor-induced PNPT1 suppresses the mtRNA-dependent immune response

We previously reported the critical role of mitochondrial RNA (mtRNA) release in antitumor immunity, and that chemotherapy activates the MAVS pathway via mtRNA release to enhance antitumor immunity. However, many patients show poor chemotherapy response and develop chemoresistance clinically. This suggests that tumors may evade the mtRNA-MAVS pathway through specific mechanisms to gain chemoresistance, despite its role in chemotherapy-induced antitumor immunity. Accordingly, this study aims to identify and elucidate the mechanisms underlying tumor escape from the mtRNA-MAVS pathway during chemoresistance development.

Due to intrinsic chemosensitivity differences across tumor cell lines, direct comparisons are confounded by genetic background and inherent biological variations. To eliminate such confounders and ensure reliable screening, we used chemosensitive and chemoresistant sublines derived from the same parental cell line. This design enables focused analysis of chemoresistance- and immune escape-related differences, minimizing inter-cell line background interference.

To identify factors contributing to resistance to antitumor therapy, we analyzed GEO datasets including multiple chemotherapy-resistant cancer cell lines. GSEA revealed that pathways related to mitochondrial gene expression were significantly enriched in

chemotherapy-resistant ovarian cancer cells (Fig. 3a). Further coupling analysis revealed that the mitochondrial gene polyribonucleotide nucleotidyltransferase 1 (PNPT1), which is involved in the mitochondrial gene expression pathway, was the only significantly upregulated gene across 3 chemotherapeutic-resistant cell lines (Fig. 3b, c). Meanwhile, the analysis indicated that in the three resistant cell lines, there was no significant change in MAVS, and the expression trend of BAX was not uniform, only PNPT1 was significantly upregulated in all resistant cells, suggesting that PNPT1 is a common gene for tumor chemotherapy resistance (Fig. S4a). While previous research highlighted PNPT1's role in mitochondrial nucleic acid metabolism [34,35], its specific influence on tumor development and therapy resistance remains unclear. Analysis of online data revealed significantly higher levels of PNPT1 mRNA in liver cancer tissue compared to nontumor tissues. Both unpaired and paired analyses revealed that PNPT1 expression was markedly elevated in liver tumor tissues compared with adjacent normal tissues in the GEO dataset (Fig. 3d). Furthermore, IHC of matched patient samples from the HPA-LIHC datasets validated the higher expression of Pnpt1 in tumor tissue (Fig. 3e). Additionally, upregulated PNPT1 expression was observed in an N-RAS/Akt-induced mouse model of primary liver cancer (Fig. 3f). These findings suggest that PNPT1 is significantly upregulated in tumor tissues, indicating its role in tumor progression. Our findings indicate that mitochondrial RNA plays a crucial role in antitumor immunity (Fig. 2), while tumors upregulate PNPT1, implies that PNPT1, as a mitochondrial RNA nuclease, may regulate the anti-tumor immune response. An analysis of IHC scores for PNPT1 and IFNA1 from HCC patients in the HPA database revealed a negative correlation between PNPT1 and IFNA1 (Fig. 3g), suggesting that PNPT1 negatively regulates interferon expression. To investigate the role of PNPT1 in regulating anticancer immunity, we generated stable cell lines expressing shRNAs targeting PNPT1 (shPNPT1-1 and shPNPT1-2). Both cell lines presented reduced PNPT1 protein levels, which remained consistently low over several generations (Fig. S4b). In B16

cells with stable shPNPT1 expression, we observed downregulation of PNPT1 mRNA and upregulation of CXCL10, IFN-β, and IL-6 mRNAs (Fig. 3h). Given that PNPT1 knockdown promotes immune responses, we hypothesized that reducing PNPT1 levels in tumors could enhance chemotherapy effectiveness. Notably, in shPNPT1 B16 cells, DOX significantly increased the mRNA expression of Cxcl10, IFN-β, IL-1β, IL-6, IL-8, and TNF-α, whereas control cells presented only slight responses (Fig. 3i). Additionally, CIPT treatment induced significantly higher levels of IFN-β, IL-1β, and IL-6 mRNA in shPNPT1 B16 cells than in control cells (Fig. 3j). In human HepG2 cells stably expressing shPNPT1, DOX significantly induced IFN-β expression, whereas control cells did not (Fig. 3k, l). These results collectively indicate that PNPT1 knockdown promotes immune responses in both mouse tumor cells and human cancer cells following chemotherapy. Our previous findings demonstrated that PNPT1 suppresses immune responses and promotes therapy resistance. We next evaluated the role of PNPT1 in regulating mitochondrial nucleic acid release and immune responses. Notably, PNPT1 knockdown led to cytoplasmic dsRNA accumulation in B16 cells (Fig. S4c). Additionally, PNPT1 knockdown increased mtRNA release into the cytoplasm of B16 cells (Fig. S4d), and this release was further amplified by DOX treatment (Fig. S4e). The same experiment also yielded the same results in HeLa cells (Fig. S4f). Lastly, PNPT1 knockdown promoted immune responses in B16 were abrogated by IMT1 treatment (Fig. S4g), indicates that the regulation of immune responses by PNPT1 depends on mtRNA. Overall, these findings suggest that tumors upregulate PNPT1 to suppress mitochondrial double-stranded RNA release, thereby attenuating immune surveillance and inhibiting chemotherapy-mediated immune responses.

PNPT1 suppresses antitumor immunity in solid tumors

The solid tumor microenvironment drives immune escape and treatment resistance,

underscoring the critical heterogeneity between tumor and normal cells[22]. Building on our discovery that tumor-induced PNPT1 suppresses mtRNA-dependent immune responses in human and murine cancer cells (Fig. 3 and S4), we have explored its role in antitumor immunity within solid tumors. Using a B16 subcutaneous tumor model—characterized as an immunologically "cold" tumor with limited immune infiltration—we implanted stable shPNPT1-expressing B16 cells into immunodeficient NSG mice and immunocompetent C57BL/6 mice (Fig. 4a). In NSG mice (severely immunodeficient mice), shPNPT1 and shNC tumors showed comparable volumes, weights, and sizes (Fig. 4b). By contrast, C57BL/6 mice bearing shPNPT1 tumors exhibited significantly reduced tumor volumes and weights relative to controls (Fig. 4c), indicating heightened sensitivity to host anticancer immunity. Notably, shPNPT1-treated tumors displayed fewer viable tumor cells and enhanced cytotoxicity (Fig. 4d), were accompanied by increased infiltration of $CD4^+$ and $CD8^+$ T cells (Fig. 4e), suggesting that PNPT1 restricts immune invasion and tumor cell killing. Analysis via the UALCAN portal revealed elevated PNPT1 expression in metastatic skin cutaneous melanoma (SKCM) and liver hepatocellular carcinoma (LIHC) tissues, with intermediate levels in primary tumors and low expression in normal tissues (Fig. 4f-g) [36]. C57BL/6 mice injected with shPNPT1-B16 cells showed markedly reduced lung metastasis, fewer metastatic clones, lower lung weights, and decreased tumor nodules (Fig. 4h-l), demonstrating that PNPT1 knockdown suppresses tumor metastasis in vivo.

To assess the role of MAVS in this antitumor response, we used shRNA targeting MAVS (shMAVS) in B16 cells, which achieved near-complete depletion of MAVS mRNA (Fig. 4m). In stable shPNPT1-expressing cells, IFN-β and IL-6 mRNA levels were significantly upregulated, an effect abrogated by shMAVS co-expression. In mice, shPNPT1-B16 tumors showed reduced growth, but this inhibition was reversed when shMAVS was co-introduced (Fig. 4n-o), indicating that MAVS knockdown counteracts the antitumor effects of PNPT1

depletion.

Building on our prior findings that mtRNA triggers antitumor immune responses and PNPT1 negatively regulates this pathway in cell and subcutaneous tumor models, we investigated in vivo immune surveillance in primary liver cancer. Using a hydrodynamic injection model of NRasV12/AKT-driven hepatocellular carcinoma (Fig. S5a), we delivered adeno-associated viruses carrying shRNA against murine PNPT1 (shmPNPT1) or control shRNA (shNC). shPNPT1 treatment significantly reduced PNPT1 mRNA and protein levels in the livers (Fig. S5b-c). Six weeks post-injection, wild-type mice developed liver tumors, whereas shPNPT1 mice showed reduced tumor burden, lower liver weights, and decreased hepatic damage (Fig. S5d-f), confirming that PNPT1 inhibition suppresses primary liver cancer development. Collectively, these data demonstrate that PNPT1 knockdown enhances anticancer immunity, restricts tumor metastasis, and suppresses tumor growth, highlighting PNPT1 as a key mediator of immune evasion and resistance to antitumor immunity.

Loss of PNPT1 overcomes therapeutic resistance

Despite significant advancements in cancer therapeutics, many malignancies develop drug resistance and evade immune surveillance, presenting substantial challenges to treatment efficacy. Previous studies have shown that tumor-induced PNPT1 expression suppresses the immune response, prompting us to further evaluate its role in therapeutic resistance.

GSEA analysis has revealed a negative correlation between PNPT1 expression and IFN-γ response pathways, which are pivotal for antitumor immune responses (Fig. 5a). Additionally, PNPT1 levels were negatively associated with CD8+ T-cell scores in patients with skin cutaneous melanoma (SKCM) (Fig. 5b). Furthermore, in SKCM, prostate adenocarcinoma (PRAD), and liver hepatocellular carcinoma (LIHC), PNPT1 expression inversely correlated with the expression of granzyme B (GZMB)[37], a key lymphocyte effector protein (Fig. 5c-e).

These findings suggest that PNPT1 suppresses lymphocyte infiltration and antitumor function within tumors.

Analysis of TCGA data has demonstrated significantly elevated PNPT1 mRNA levels in various common tumors compared to non-tumor tissues. Both unpaired and paired analyses confirmed markedly higher PNPT1 expression in tumor tissues versus adjacent normal tissues (Fig. S6a). Consistently, CPTAC data showed elevated PNPT1 protein levels in tumors relative to non-tumor tissues (Fig. S6b). Lower PNPT1 expression was associated with favorable prognoses in LIHC patients (Fig. S6c) and in adrenal cortex carcinoma (ACC), esophageal carcinoma (ESCA), chromophobe renal cell carcinoma (KICH), and low-grade glioma (LGG) (Fig. S6d). Collectively, these results indicate that PNPT1 expression correlates positively with cancer incidence and progression.

Given the close relationship between tumor immune infiltration and antitumor therapy efficacy, we investigated how PNPT1 modulation affects cancer treatment. Following DOX administration, tumor volume remained stable in shNC-treated groups, whereas shPNPT1-treated tumors showed significant regression (Fig. 5f). In C57BL/6 mice, shPNPT1 combined with DOX for 14 days led to marked reductions in tumor weight and volume (Fig. 5g). Flow cytometry revealed increased tumor-infiltrating lymphocytes (TILs), including CD4+ and CD8+ T cells, in PNPT1-knockdown tumors after DOX treatment (Fig. 5h). These findings indicate that PNPT1 knockdown enhances DOX-mediated tumor growth inhibition, highlighting its role as a chemotherapeutic resistance factor and its negative correlation with immune cell infiltration.

Finally, we evaluated the impact of PNPT1 on PD-1 checkpoint blockade therapy. While PD-1 blockade has shown limited efficacy in solid tumors[38,39], shPNPT1-treated tumors exhibited reduced volume compared to shNC controls. Notably, the combination of shPNPT1 and PD-1 antibody treatment synergistically inhibited tumor growth, whereas single-agent

367 treatments showed modest effects (Fig. 5i-k). Tumor weights in the combined treatment group
368 were significantly lower than in all other groups, demonstrating that PNPT1 knockdown
369 enhances the efficacy of PD-1 antibody therapy.

370 Collectively, these results establish that PNPT1 suppresses antitumor immune responses
371 and promotes tumor progression. Moreover, PNPT1 knockdown overcomes resistance to both
372 chemotherapy and immune checkpoint blockade, positioning PNPT1 as a potential therapeutic
373 target to enhance cancer treatment efficacy.

374

375

376 **Pharmacological inhibition of PNPT1 synergizes with the BH3 mimetic drugs results in**
377 **robust antitumor immunity and overcomes therapeutic resistance**

378 Our previous findings suggest that mtRNA efficiently activates antitumor immunity,
379 whereas the tumor microenvironment upregulates PNPT1 to inhibit this response. As noted
380 previously, the clinical translation of STING agonists has been substantially hindered. To date,
381 no therapeutics targeting the mRNA-MAVS signaling axis have been reported. In response to
382 this unmet need, we have pioneered a novel therapeutic strategy targeting the PNPT1-mtRNA
383 axis. We first investigated lanatoside C (Lanc), an FDA-approved drug clinically used for
384 treating chronic heart failure that was recently reported to inhibit PNPT1 [40], however, its role
385 in antitumor therapy has not been proven. While Lanc induced a weak immune response in
386 macrophages, it had little effect on tumor cells, indicating that simply inhibiting PNPT1 may
387 not be sufficient (Fig. S7a-c). One possible reason for the ineffectiveness of PNPT1 inhibitors
388 alone is the overexpression of antiapoptotic BCL-2 family members (such as BCL-2, BCL-XL,
389 and MCL-1) in tumor cells and tissues[41,42], which prevent the formation of BAK/BAX pores
390 necessary for mtRNA release (Fig. 2). Therefore, we designed a combination therapy using
391 BH3-mimetic drugs[43-45], which inhibit the survival of BCL-2 family members and promote

apoptosis by opening BAK/BAX pores (Fig. 6a). This class of drugs has been clinically used to treat blood cancers, but it is less effective against solid tumors. We selected Navitoclax (ABT-263) and Venetoclax (ABT-199) for our study. The former targets several antiapoptotic proteins, such as BCL-2, BCL-XL, and BCL-W, while the latter, already approved by the FDA, is used to treat chronic lymphocytic leukemia (CLL) and acute myelocytic leukemia (AML)[43,46]. While neither Lanc nor BH3-mimetic drugs alone activated an immune response, their combination significantly induced one (Fig. 6b). Notably, ABT-263 demonstrated enhanced efficacy, potentially due to its broader targeting spectrum. The combined treatment further amplified the immune response triggered by DOX (Fig. 6c, d) and facilitated mtRNA release into the cytoplasm (Fig. 6e), with similar results observed in macrophages (Fig. 6f-h). This combination also effectively induced immune responses in various human cancer cells (Fig. 6i, j). Crucially, the combination did not compromise the apoptosis-inducing ability of BH3-mimetic drugs (Fig. S7d) and maintained their tumor-killing efficacy (Fig. S7e, f). These results indicate that combining BH3-mimetic drugs with the Lanc significantly activates the antitumor immune response while preserving the tumoricidal effects of BH3 mimetics.

We further tested the efficacy of the drug combination (ABT-263 + Lanc) in vivo using immunocompetent C57BL/6 mice implanted with B16 cells (Fig. 6k). The results indicated that while single drug treatments had limited effects, the combination significantly inhibited tumor growth (Fig. 6l-o). Remarkably, even at reduced dosage, substantial antitumor effects were still produced (Fig. 6l). Furthermore, the combined treatment inhibited tumor growth, reduced tumor size, and significantly prolonged survival (Fig. 6m-o). Additionally, this combination enhanced immune responses within the tumor tissue (Fig. 6p), and tumors presented fewer tumor cells, greater cytotoxicity and greater CD8+ T-cell infiltration in drug-treated tumors than in control tumors (Fig. 6q). Throughout the treatment course, the combination only slightly affected the body weight of the mice initially; however, the body

weight returned to control levels thereafter (Fig. S7g). Pathological assessments revealed no significant organ damage from the treatments (Fig. S7h), confirming the safety of the drug combination in mice model. The alternative combination of ABT-199 and Lanc also resulted in tumor growth inhibition and significantly prolonged survival (Fig. 6r-t). In a clinical context where multimodal therapies are common, we observed that tumor volume remained largely unchanged with DOX or anti-PD-1 monotherapy. However, combining ABT-263 + Lanc significantly reduced tumor volume when combined with these treatments and significantly prolonged survival (Fig. 6u-w). These results suggest that the ABT-263 + Lanc combination can effectively overcome cancer resistance to anti-cancer therapy. Finally, we evaluated the potential of the combination drugs in treating primary liver cancer (Fig. 6x). The control mice developed liver tumors, whereas those treated with the combination presented a reduced tumor presence, significantly lower liver weights and significantly prolonged survival (Fig. 6y), and a reduced liver damage area (Fig. 6z), indicating that the combination effectively suppressed primary liver cancer development.

Our results highlight several advantages of the combination drug approach. First, Lanc inhibits PNPT1 and promotes the production of immunogenic mtRNA, whereas BH3-mimetic drugs effectively open BAK/BAX pores, facilitating mtRNA release into the cytoplasm to activate immune responses. Second, Lanc alone has poor antitumor effects, and while BH3-mimetic drugs are effective in hematologic tumors, they are less effective in solid tumors because of their immunosuppressive apoptotic effects, which can induce tumor antigen tolerance[47-49]. By combining these drugs, we not only preserve the tumor-killing ability of BH3 mimetics but also effectively enhance the immune response, transforming "cold" tumors into "hot" tumors. This strategy overcomes the limitations of individual therapies, significantly improving overall antitumor efficacy, and both drugs have previously been approved for clinical use with good safety profiles. In summary, our data confirm that pharmacological

inhibition of PNPT1 synergizes with BH3-mimetic drugs to induce robust antitumor immunity and overcome therapeutic resistance in solid tumors, highlighting that this combinatorial approach holds considerable promise for clinical translation.

Discussion

The innate immune system serves as the body's indispensable first line of defense against microbial pathogens, while also maintaining tissue homeostasis. It rapidly activates in response to pathogen-associated molecular patterns (PAMPs) and damage-associated molecular patterns (DAMPs), orchestrating immune clearance mechanisms. Beyond infections, the body confronts diverse stressors—including DNA damage, oxidative stress, and oncogene activation[50]—that can lead to the accumulation of damaged cells, elevating cancer risk. Thus, effective immune activation under such stressful conditions is critical for eliminating aberrant cells and preventing malignant transformation. Innate immunity also plays a pivotal role in tumor therapy: radiotherapy and chemotherapy enhance cancer patient survival not only by directly eradicating tumor cells but also by potentiating immune responses and sensitizing tumors to immunotherapies [12]. However, the mechanisms underlying immune activation during antitumor therapies require deeper exploration to unlock their full therapeutic potential.

Our research illuminates the central role of mitochondria-derived nucleic acids in triggering immune responses during antitumor interventions. Chemotherapy induces the release of mitochondrial RNA (mtRNA) into the cytoplasm, a process that activates innate immunity through the formation of double-stranded RNA (dsRNA) structures. In normal cells, dsRNA is compartmentalized within mitochondria, preventing autoimmunity while priming the cell for rapid immune responses to future stimuli. During chemotherapy, mitochondrial dsRNA is released via BAX/BAK channels, activating the MAVS signaling

pathway and inducing the expression of interferons and inflammatory factors. This immune cascade is essential for recruiting immune cells and facilitating tumor clearance.

Notably, the cGAS-STING signaling pathway—traditionally targeted for its role in detecting tumor DNA[51-53]—has faced therapeutic challenges. Evidence shows STING expression is downregulated in numerous tumor types, and certain chemotherapies fail to activate this pathway, highlighting the limitations of targeting cGAS-STING alone [13-15,19]. In contrast, the widespread expression of MAVS-related components across tumor tissues suggests that mitochondrial RNA-derived danger signals can effectively trigger antitumor immunity in a broad range of cancers.

Tumor microenvironments exist in a state of heightened stress due to intrinsic metabolic dysregulation and environmental pressures, enabling tumors to suppress immune responses and evade surveillance [20-22]. While chemotherapeutic agents induce cellular stress to exert antitumor effects, solid tumors often exhibit profound drug resistance, reflecting their functional heterogeneity compared to normal cells. Our findings reveal that the mitochondrial RNA metabolic enzyme PNPT1 is upregulated in tumor tissues, where it specifically inhibits the formation and release of immunogenic mitochondrial dsRNA, thereby suppressing innate immunity and immune-mediated clearance. Knocking down PNPT1 in both normal and tumor cells enhances dsRNA release, accelerating immune elimination of damaged cells. Clinical data confirm elevated PNPT1 RNA and protein levels in various malignancies, implicating PNPT1 in dampening antitumor immune responses. In vivo studies further demonstrate that reducing PNPT1 inhibits tumor growth and synergizes with chemotherapy and immune checkpoint therapies, underscoring its role in promoting tumor progression and therapeutic resistance.

In summary, our research uncovers a novel mechanism whereby mitochondrial nucleic acids act as stress-associated molecular patterns during tumorigenesis and antitumor therapy,

triggering immune surveillance and clearance. The formation and release of mitochondrial dsRNA emerge as key drivers of innate immune activation in response to stress and infection. Malignant cells counteract this by upregulating PNPT1, which suppresses dsRNA-mediated signaling to facilitate immune evasion and treatment resistance. Critically, pharmacological inhibition of PNPT1 in combination with BH3-mimetic drugs potently activates mtRNA-mediated antitumor immunity, overcoming resistance in solid tumors without systemic toxicity. These findings establish a promising combinatorial strategy to enhance cancer immunotherapy with potential for safe and effective clinical translation.

Materials and Methods

Key resources table

Antibodies	Source	Cat NO.
Anti-p-TBK1	Abcam	ab109272
Anti-TBK1	Abcam	ab40676
Anti-PNPT1	proteintech	14487-1-AP
Anti- dsRNA J2	Scicons	10010200
Anti-GAPDH	Sigma-Aldrich	G9295
Anti-Flag	Sigma-Aldrich	F3165
Anti-Mouse IgG Dylight649	Abbkine	A23610
Anti-Rabbit IgG Dylight649	Abbkine	A23620
Anti-Rabbit IgG FITC	Abbkine	A22120
Anti-Mouse IgG FITC	proteintech	20000029
Anti- S9.6	Antibody System	RGK60001
Anti-Rabbit IgG CY3	Abbkine	A22220
Anti- Mouse IgG CY3	Abbkine	A22210
Anti-TOM20	Abclone	A6744
Anti-TOM20	Abclone	A19403
Anti-CD4	Abcam	ab183685
Anti-CD8	Abcam	ab217344
Anti-F4/80	Abcam	ab300421
PD-1 antibody	Bio x cell	BE0273

Experimental Models: Cell Lines	Source	Cat NO.
HEK293T	ATCC	Cat#: CRL-3216
HeLa	ATCC	Cat#: CCL-2
WT MEF	This paper	N/A
MAVS-/- MEF	This paper	N/A
WI-38	ATCC	CRL - 7728
B16	CTCC	GDC038
Vero	CTCC	GDC029

518

Virus and bacterial strain	Source	Cat NO.
E. coli DH5α	TRANSGEN	Cat#: CD201
VSV	From Dr. Bo Zhong, Wuhan University	N/A
Plko.1-shCrtl, Plko.1-shpnpt1 Plko.1-shMAVS lentivirus	This paper	N/A

519

Chemicals and reagent	Source	Cat NO.
IMT1	Targetmol	2304621-31-4
N-acetylcysteine	Targetmol	16-91-1

BAY 11-7082	Targetmol	19542-67-7
lipofectamine 2000	Invitrogen	11668500
Poly(I:C)	invivogen	tlrl-pic
Etoposide	Targetmol	33419-42-0
Si-RNA(si-control/ si-PNPT1)	Ribobio	N/A
Doxorubicin	Targetmol	23214-92-8
MitoTracker Red	Thermo Fisher Scientific	M22426
Digitonin	Sigma	11024-24-1
Cyclosporin A	MCE	59865-13-3
Bax inhibitor peptide V5	MCE	579492-81-2
Cisplatin	Targetmol	15663-27-1
Mouse IFN-β ELISA kit	Biolegend	43940b

520

Experimental Models:	Source	Cat NO.

Organisms/Strains		
Mouse: C56BL/6 Mavs−/−	From Dr. Hongbin Shu, Wuhan University	N/A

Software		
DNAMAN	Lynnon	https://www.lynnon.com
GraphPad Prism 9	Biosoft	https://www.graphpad.com
Primer Premier 5	GraphPad	http://www.premierbiosoft.com/primerdesign/
Las x	Leica	https://www.leica-microsystems.com.cn/

Animal study

C57BL/6 WT mice were obtained from the Hubei Research Center of Laboratory Animals (Wuhan, China). MAVS$^{-/-}$ mice on a C57BL/6 background were generously provided by Dr. Hongbin Shu from Wuhan University (Wuhan, China). NSG mice were sourced from Gempharmattech Co., Ltd (Nanjing, China). All animal experiments were approved by the IACUC of the College of Life Sciences, Wuhan University. The studies adhered to the Animal Welfare Act and the National Institutes of Health guidelines for the care and use of experimental animals in biomedical research.

For the CIPT experiment, six- to eight-weeks-old mice were intraperitoneally injected with 15-25 mg/kg of Cisplatin and monitored daily for durability. After 48–72 hours, serum samples were collected from the mice to assess indicators of inflammatory response and organ damage. Additionally, mouse tissues were harvested for immunohistochemistry and quantitative real-time PCR (qRT-PCR) analyses.

For tumor challenge, 5×10^5-2×10^6 B16 cells were suspended in Hanks balanced salt solution and subcutaneously injected into the C57 mice right underarm on day 0. For NSG mice, 2×10^5 B16 cells were suspended in Hanks balanced salt solution and subcutaneously injected to the right underarm on day 0. After the initial formation of the tumor, the length and width of the tumor were tested every two days until the end of the experiment. For the tumor chemotherapy experiment, the mice were injected with 4 mg/kg DOX intraperitoneally on the 6^{th} and 9^{th} day, respectively. For the immune checkpoint blocking experiment, the mice were intraperitoneally injected with 100 μg PD-1 antibody on days 6, 9 and 12. The tumor volume was estimated using the formula (length×width×width)/2. After euthanasia, tumor tissues were harvested for immunohistochemistry and flow cytometry analyses.

Mouse liver cancer was induced by hydrodynamic injection of Sleep Beauty transposon-overexpressing myr-AKT/NRASV12, each mice were injected with plasmid contain pT3-myr-AKT-HA (10 μg), pT/Caggs-NRASV12 (10μg), and pCMV (CAT)T7-SB100 (2 μg), after 6-12 days , mice liver were harvested for immunohistochemistry and quantitative immune cell infiltration and N-Ras clearance. After 5-8 weeks, the livers were harvested for immunohistochemistry and quantitative assessment of cancer progression.

For immunohistochemical experiments, the different organs of mice were fixed in 4% paraformaldehyde, embedded in paraffin, sectioned and stained with stain or antibody, then observed under a microscope.

For the flow cytometry experiment, the mice's tumor tissues were cut, digested with collagenase at 37°C for 30 minutes, and the cell suspension was separated. The number of cells was counted, stained with antibodies, then analyzed on a flow cytometer (Beckman).

Cell and cultures and treament

HeLa cells, MEFs, Vero cells and HEK293 cells were cultured in Dulbecco's modified

Eagle's medium (DMEM) (Gibco, Grand Island, NY, USA) supplemented with 10% Fetal Bovine Serum (FBS), 100 U/ml penicillin, and 100 μg/ml streptomycin sulfate. All cells were cultured in an incubator at 37°C in 5% CO_2.

For drug treatment, cells at approximately 60–70% confluency were treated with 0–5 μM Dox, 0–20 μM cisplatin and 0–100 μM H_2O_2 for 6–24 h, which were then collected for subsequent analysis.

Lentivirus

Plko.1-shCrtl, Plko.1-shPNPT1 and Plko.1-shMAVS were constructed, and the stably expressed viral products were generated. In short, the constructed plasmid and packaging plasmid were transfected into HEK293T cells. After 48 h, the cell supernatant was collected, and then filtered with a 0.45 um filter to obtain lentivirus, which was used to infect the target cells for 48 h. Puromycin was used to screen positive cells. The sequence of shRNA was obtained from Sigma.

Immunoblotting

Cells were lysed in a buffer containing 50 mm Tris-HCl (pH7.5), 0.5 mm EDTA, 150 mM NaCl, 1% NP40 and 1% SDS, then protease inhibitor and a phosphatase inhibitor (Roche) were added to the lysate, which was briefly ultrasonicated or overturned at 4°C for 1 h and centrifuged to collect the supernatant. Then, protein buffer was added to the supernatant for electrophoresis, denatured at 100°C for 5 min, and SDS-PAGE was used for electrophoresis. Following this, the membrane was transferred, and indicated antibodies were used to detect the target protein.

Monoclonal mouse anti-GAPDH (G9295, Sigma), anti-PNPT1 (14487-1-AP, Proteintech) and dsRNA J2 antibody (10010200, Scicons) were purchased from indicated

manufacturers. Anti-Rabbit IgG FITC, Anti-Mouse IgG FITC, Anti-Mouse IgG CY3 and Anti-Rabbit IgG CY3 were purchased from Abbkine. MitoTracker Red (M22426, Thermo Fisher Scientific) and Digitonin (D141, Sigma) were purchased from indicated manufacturers. Lipofectamine 2000, normal rabbit immunoglobulin G (IgG). Etoposide, Doxorubicin, and Cisplatin were purchased from Targemol (USA). Poly(I:C) was purchased from Invivogen (USA).

qRT-PCR and ELISA

Total RNAs were isolated from the tissues or cells using Trizol reagent (Invitrogen). Then, cDNA was generated from 1 μg of isolated RNA by reverse transcription with a reverse transcription mix (Vazyme Biotech Co., Ltd, China). Specific primers and ChamQ SYBR qPCR Master Mix (Vazyme Biotech Co., Ltd, China) were used for the RT-PCR reactions. For ELISA experiments, an ELISA kit was used to determine the levels of cytokines in cell supernatant or mouse serum. All subsequent experimental steps were performed according to the manufacturer's instructions.

Immunofluorescence and confocal microscopy analysis

Cells were cultured in confocal dishes for 24–48 h, after which the supernatant was removed and the cells were fixed with 4% paraformaldehyde for 15 minutes. Following three washes with PBS, 0.1% Triton X-100 was added to permeabilize the cell membrane for 5 minutes, then the cells were blocked with 5% BSA for 45 minutes. A specific primary antibody was added and the cells were kept at 4° C overnight. After washing, the cells were incubated with a secondary antibody for 1 hour and then washed three times. The nuclei were labeled with DAPI (1 μg/ml), after which the cells were observed under a confocal microscope.

Mitochondrial extraction and mtRNA treatment

Mitochondria were isolated from cultured cells using a Mitochondrial Isolation Kit (Thermo Scientific, 89874). Trizol reagent was added to the purified mitochondria to extract RNA from the mitochondria. After obtaining mitochondrial RNA, a total amount of 2–5 μg mtRNA was transfected into new untreated cells. After 12 h, the treated cells' RNAs were extracted for subsequent analysis. RNase III (M0245S, NEB) was used for the RNase treatment experiment to treat mtRNA according to the reagent instructions, followed by RNase treatment mtRNA transfection and analysis based on the above steps.

Detection of mtRNA in cytosolic extracts and cytosolic RNA treatment

The digitonin extraction method was used to extract cytosolic RNA. Briefly, the cells were treated with digitonin (20 μg/ml). The purity of the cytosolic components was detected by Western blot. Then, the cytosolic RNA was extracted, and mtRNA-specific primers were used for qPCR. For the cytosolic RNA treatment experiment, a total amount of 2–5 μg cytosolic RNA was transfected into new untreated cells. After 12 h, RNAs were extracted from the treated cells for subsequent analysis.

For the RNase treatment experiment, RNase III (M0245S, NEB) and RNase H (D7089, Beyotime) was used to treat cytosolic RNA and R-loop according to the Manufactures' instructions, and then RNase treated cytosolic RNA and R-loop were transfected and analyzed according to the above steps.

Immunoprecipitation of cytoplasm mtdsRNA and mt R-loop

Cells were treated with digitonin (20 μg/ml). Cell lysate was prepared and transferred to 1.5 ml of a fresh RNA-free enzyme tube and centrifuged at 4℃ at 12000 rpm for 10 min. The

supernatant was transferred to a fresh tube, dsRNA J2 and R-loop S9.6 antibody was added and kept on a rotor at 4℃ for 1–2 h. The sample tubes were added with Protein G and then kept on the rotor at 4℃ for 2 h, centrifuged. The supernatant was removed, washed twice, and a J2 antibody bound dsRNA was extracted with Trizol reagent, 9.6 antibody bound R-loop were isolation by phenol chloroform extraction, then mtdsRNA and mt R-loop was detected by qPCR using the mtRNA specific primers.

ROS detection

A ROS Kit (Beyotime, s0033s) was used to detect ROS in the cultured cells (>10,000 cells) using flow cytometry (FCM) following the manufacturer's instructions.

TCGA data and online data analysis

Gene expression profiles of patient samples were downloaded from the TCGA dataset (https://portal.gdc.cancer.gov/). Clinical data were downloaded from the University of California Santa Cruz Xena dataset (http://xena.ucsc.edu/). Patient proteome data were obtained from the CPTAC dataset (https://proteomic.datacommons.cancer.gov/pdc/). RNA-Seq data of drug-resistant cell lines (GSE270030, GSE140077, GSE222187) and drug-treated cell lines (GSE223698, GSE81878, GSE235908, GSE108214) were available on the GEO database (http://www.ncbi.nlm.nih.gov/geo). We analyzed the expression of multiple nucleic acid sensors in different tissues or cell types using public databases such as The Human Protein Atlas (HPA). Gene expression levels in different tissue cells were obtained from the Human Protein Atlas. We used the RNA dataset from the Human Protein Atlas, including RNA single-cell type data and RNA HPA tissue gene data. IHC data from HPA were available on the website (http://www.proteinatlas.org/). The RNA-Seq data were normalized using the DESeq2 package or converted to TPM values. The immune cell infiltration levels of each

SKCM sample were evaluated using Cibersortx (https://cibersortx.stanford.edu/). For gene-set enrichment analysis, the gene expression matrix of SKCM was divided into two parts based on the PNPT1 expression level. The pre-ranked data were uploaded to GSEA 4.1.0, and the enrichment of MSigDB C2 gene sets was analyzed with 1,000 random permutations to obtain P values, q values, and NES. For analyzing the association of PNPT1 expression with survival and tumor metastasis, the online UALCAN portal (http://ualcan.path.uab.edu/) and GEPIA (http://gepia.cancer-pku.cn/about.html) were used to assess the impact of PNPT1 expression on patient survival rates and metastasis.

Statistical analysis

The related results were expressed as the mean ± standard error of the mean (SEM) or standard deviation (SD). Statistical methods are described in detail in the figure legend. The Prism v9 software was used for statistical analysis. P value <0.05 was statistically significant.

Acknowledgements

We thank Professor Hongbing Shu of Wuhan University, China, for kindly providing C57BL/6 MAVS$^{-/-}$ mice. We appreciate Associate Professor Kaisa Cui of Jiangnan University, China, for generously sharing their experience and suggestion. We thank Qian Liu from the animal Experimental center for technical support. This work was supported by National Natural Science Foundation of China (32188101, 32400131), National Key Research and Development Program of China (2023YFC2306600), and China Postdoctoral Science Foundation (2024T170687, 2024M752482, GZB20230541).

Author Contributions

685 Ke Lan, Kailang Wu, and Mingfu Tian conceived the study. Mingfu Tian, Siyu Liu, Zelin
686 Chai, Zhiqiang Li, and Hong Fan designed, performed, and analyzed experiments and
687 interpreted data. Mingfu Tian, Siyu Liu, and Xu Li performed and analyzed experiments. Xu
688 Li performed bioinformatic analyses. Chengliang Zhu contributed to the reagents. Kailang
689 Wu and Ke Lan supervised the experiments. Mingfu Tian, Kailang Wu, and Ke Lan
690 contributed to the writing the paper. Mingfu Tian, Kailang Wu, and Ke Lan contributed to the
691 editing the paper.

692

693 **Competing interests**

694 Authors declare that they have no competing interests.

695

696 **Data and materials availability**

697 All data are available in the main text or the supplementary materials.

698

699 **References**

700

701 1 Akira, S., Uematsu, S. & Takeuchi, O. Pathogen recognition and innate immunity.
702 *Cell* **124**, 783-801, doi:10.1016/j.cell.2006.02.015 (2006).
703 2 Gong, T., Liu, L., Jiang, W. & Zhou, R. DAMP-sensing receptors in sterile
704 inflammation and inflammatory diseases. *Nature reviews. Immunology* **20**, 95-112,
705 doi:10.1038/s41577-019-0215-7 (2020).
706 3 Man, S. M. & Kanneganti, T. D. Innate immune sensing of cell death in disease and
707 therapeutics. *Nat Cell Biol* **26**, 1420-1433, doi:10.1038/s41556-024-01491-y (2024).
708 4 Pradeu, T., Thomma, B., Girardin, S. E. & Lemaitre, B. The conceptual foundations of
709 innate immunity: Taking stock 30 years later. *Immunity* **57**, 613-631,
710 doi:10.1016/j.immuni.2024.03.007 (2024).
711 5 Bowie, A. G. & Unterholzner, L. Viral evasion and subversion of pattern-recognition
712 receptor signalling. *Nature reviews. Immunology* **8**, 911-922, doi:10.1038/nri2436
713 (2008).
714 6 Demaria, O. *et al.* Harnessing innate immunity in cancer therapy. *Nature* **574**, 45-56,
715 doi:10.1038/s41586-019-1593-5 (2019).
716 7 Cao, L. L. & Kagan, J. C. Targeting innate immune pathways for cancer
717 immunotherapy. *Immunity* **56**, 2206-2217, doi:10.1016/j.immuni.2023.07.018 (2023).

8 Huang, Y. *et al.* Myeloid PTEN promotes chemotherapy-induced NLRP3-inflammasome activation and antitumour immunity. *Nat Cell Biol* **22**, 716-727, doi:10.1038/s41556-020-0510-3 (2020).

9 Hu, A. *et al.* Harnessing innate immune pathways for therapeutic advancement in cancer. *Signal transduction and targeted therapy* **9**, 68, doi:10.1038/s41392-024-01765-9 (2024).

10 Vacchelli, E. *et al.* Chemotherapy-induced antitumor immunity requires formyl peptide receptor 1. *Science* **350**, 972-978, doi:10.1126/science.aad0779 (2015).

11 Lanng, K. R. B., Lauridsen, E. L. & Jakobsen, M. R. The balance of STING signaling orchestrates immunity in cancer. *Nat Immunol* **25**, 1144-1157, doi:10.1038/s41590-024-01872-3 (2024).

12 Woo, S. R. *et al.* STING-dependent cytosolic DNA sensing mediates innate immune recognition of immunogenic tumors. *Immunity* **41**, 830-842, doi:10.1016/j.immuni.2014.10.017 (2014).

13 de Queiroz, N., Xia, T., Konno, H. & Barber, G. N. Ovarian Cancer Cells Commonly Exhibit Defective STING Signaling Which Affects Sensitivity to Viral Oncolysis. *Molecular cancer research : MCR* **17**, 974-986, doi:10.1158/1541-7786.mcr-18-0504 (2019).

14 Wu, M. J. *et al.* Mutant IDH1 inhibition induces dsDNA sensing to activate tumor immunity. *Science* **385**, eadl6173, doi:10.1126/science.adl6173 (2024).

15 Wu, L. *et al.* KDM5 histone demethylases repress immune response via suppression of STING. *PLoS biology* **16**, e2006134, doi:10.1371/journal.pbio.2006134 (2018).

16 Kottakis, F. *et al.* LKB1 loss links serine metabolism to DNA methylation and tumorigenesis. *Nature* **539**, 390-395, doi:10.1038/nature20132 (2016).

17 Konno, H. *et al.* Suppression of STING signaling through epigenetic silencing and missense mutation impedes DNA damage mediated cytokine production. *Oncogene* **37**, 2037-2051, doi:10.1038/s41388-017-0120-0 (2018).

18 Lee, K. M. *et al.* Epigenetic Repression of STING by MYC Promotes Immune Evasion and Resistance to Immune Checkpoint Inhibitors in Triple-Negative Breast Cancer. *Cancer immunology research* **10**, 829-843, doi:10.1158/2326-6066.cir-21-0826 (2022).

19 Takaki, T., Millar, R., Hiley, C. T. & Boulton, S. J. Micronuclei induced by radiation, replication stress, or chromosome segregation errors do not activate cGAS-STING. *Mol Cell* **84**, 2203-2213.e2205, doi:10.1016/j.molcel.2024.04.017 (2024).

20 Binnewies, M. *et al.* Understanding the tumor immune microenvironment (TIME) for effective therapy. *Nature medicine* **24**, 541-550, doi:10.1038/s41591-018-0014-x (2018).

21 Jiang, X. *et al.* Role of the tumor microenvironment in PD-L1/PD-1-mediated tumor immune escape. *Mol Cancer* **18**, 10, doi:10.1186/s12943-018-0928-4 (2019).

22 Cervantes-Villagrana, R. D., Albores-García, D., Cervantes-Villagrana, A. R. & García-Acevez, S. J. Tumor-induced neurogenesis and immune evasion as targets of innovative anti-cancer therapies. *Signal transduction and targeted therapy* **5**, 99, doi:10.1038/s41392-020-0205-z (2020).

23 Jackson, S. P. & Bartek, J. The DNA-damage response in human biology and disease. *Nature* **461**, 1071-1078, doi:10.1038/nature08467 (2009).

24 Uhlén, M. *et al.* Proteomics. Tissue-based map of the human proteome. *Science* **347**, 1260419, doi:10.1126/science.1260419 (2015).

25 Vazquez, C. & Horner, S. M. MAVS Coordination of Antiviral Innate Immunity. *J Virol* **89**, 6974-6977, doi:10.1128/jvi.01918-14 (2015).

26 Xu, L. G. *et al.* VISA is an adapter protein required for virus-triggered IFN-beta signaling. *Mol Cell* **19**, 727-740, doi:10.1016/j.molcel.2005.08.014 (2005).
27 Kolakofsky, D., Kowalinski, E. & Cusack, S. A structure-based model of RIG-I activation. *RNA (New York, N.Y.)* **18**, 2118-2127, doi:10.1261/rna.035949.112 (2012).
28 Tan, B. G., Gustafsson, C. M. & Falkenberg, M. Mechanisms and regulation of human mitochondrial transcription. *Nature reviews. Molecular cell biology* **25**, 119-132, doi:10.1038/s41580-023-00661-4 (2024).
29 Bonekamp, N. A. *et al.* Small-molecule inhibitors of human mitochondrial DNA transcription. *Nature* **588**, 712-716, doi:10.1038/s41586-020-03048-z (2020).
30 Fisch, D. *et al.* Molecular definition of the endogenous Toll-like receptor signalling pathways. *Nature* **631**, 635-644, doi:10.1038/s41586-024-07614-7 (2024).
31 Schönborn, J. *et al.* Monoclonal antibodies to double-stranded RNA as probes of RNA structure in crude nucleic acid extracts. *Nucleic acids research* **19**, 2993-3000, doi:10.1093/nar/19.11.2993 (1991).
32 McArthur, K. *et al.* BAK/BAX macropores facilitate mitochondrial herniation and mtDNA efflux during apoptosis. *Science* **359**, doi:10.1126/science.aao6047 (2018).
33 Wang, P. *et al.* ANT2 functions as a translocon for mitochondrial cross-membrane translocation of RNAs. *Cell research* **34**, 504-521, doi:10.1038/s41422-024-00978-5 (2024).
34 Wang, G. *et al.* PNPASE regulates RNA import into mitochondria. *Cell* **142**, 456-467, doi:10.1016/j.cell.2010.06.035 (2010).
35 Silva, S., Camino, L. P. & Aguilera, A. Human mitochondrial degradosome prevents harmful mitochondrial R loops and mitochondrial genome instability. *Proceedings of the National Academy of Sciences of the United States of America* **115**, 11024-11029, doi:10.1073/pnas.1807258115 (2018).
36 Chandrashekar, D. S. *et al.* UALCAN: An update to the integrated cancer data analysis platform. *Neoplasia (New York, N.Y.)* **25**, 18-27, doi:10.1016/j.neo.2022.01.001 (2022).
37 Cullen, S. P., Adrain, C., Lüthi, A. U., Duriez, P. J. & Martin, S. J. Human and murine granzyme B exhibit divergent substrate preferences. *The Journal of cell biology* **176**, 435-444, doi:10.1083/jcb.200612025 (2007).
38 Dermani, F. K., Samadi, P., Rahmani, G., Kohlan, A. K. & Najafi, R. PD-1/PD-L1 immune checkpoint: Potential target for cancer therapy. *Journal of cellular physiology* **234**, 1313-1325, doi:10.1002/jcp.27172 (2019).
39 Andrews, L. P., Yano, H. & Vignali, D. A. A. Inhibitory receptors and ligands beyond PD-1, PD-L1 and CTLA-4: breakthroughs or backups. *Nat Immunol* **20**, 1425-1434, doi:10.1038/s41590-019-0512-0 (2019).
40 Qu, S. *et al.* Blockade of pan-viral propagation by inhibition of host cell PNPT1. *Int. J. Antimicrob. Agents* **63**, doi:10.1016/j.ijantimicag.2024.107124 (2024).
41 Czabotar, P. E. & Garcia-Saez, A. J. Mechanisms of BCL-2 family proteins in mitochondrial apoptosis. *Nat. Rev. Mol. Cell Biol.* **24**, 732-748, doi:10.1038/s41580-023-00629-4 (2023).
42 Delbridge, A. R. D., Grabow, S., Strasser, A. & Vaux, D. L. Thirty years of BCL-2: translating cell death discoveries into novel cancer therapies. *Nat. Rev. Cancer* **16**, 99-109, doi:10.1038/nrc.2015.17 (2016).
43 Diepstraten, S. T. *et al.* The manipulation of apoptosis for cancer therapy using BH3-mimetic drugs. *Nat. Rev. Cancer* **22**, 45-64, doi:10.1038/s41568-021-00407-4 (2021).
44 Walensky, L. D. Targeting BAX to drug death directly. *Nat. Chem. Biol.* **15**, 657-665, doi:10.1038/s41589-019-0306-6 (2019).

45 Czabotar, P. E., Lessene, G., Strasser, A. & Adams, J. M. Control of apoptosis by the BCL-2 protein family: implications for physiology and therapy. *Nat. Rev. Mol. Cell Biol.* **15**, 49-63, doi:10.1038/nrm3722 (2013).

46 Merino, D. *et al.* BH3-Mimetic Drugs: Blazing the Trail for New Cancer Medicines. *Cancer Cell* **34**, 879-891, doi:10.1016/j.ccell.2018.11.004 (2018).

47 Galluzzi, L., Buqué, A., Kepp, O., Zitvogel, L. & Kroemer, G. Immunogenic cell death in cancer and infectious disease. *Nat. Rev. Immunol.* **17**, 97-111, doi:10.1038/nri.2016.107 (2016).

48 Kazama, H. *et al.* Induction of Immunological Tolerance by Apoptotic Cells Requires Caspase-Dependent Oxidation of High-Mobility Group Box-1 Protein. *Immunity* **29**, 21-32, doi:10.1016/j.immuni.2008.05.013 (2008).

49 Waldman, A. D., Fritz, J. M. & Lenardo, M. J. A guide to cancer immunotherapy: from T cell basic science to clinical practice. *Nat. Rev. Immunol.* **20**, 651-668, doi:10.1038/s41577-020-0306-5 (2020).

50 Lei, Y. *et al.* Cooperative sensing of mitochondrial DNA by ZBP1 and cGAS promotes cardiotoxicity. *Cell* **186**, 3013-3032.e3022, doi:10.1016/j.cell.2023.05.039 (2023).

51 Deng, L. *et al.* STING-Dependent Cytosolic DNA Sensing Promotes Radiation-Induced Type I Interferon-Dependent Antitumor Immunity in Immunogenic Tumors. *Immunity* **41**, 843-852, doi:10.1016/j.immuni.2014.10.019 (2014).

52 Lanng, K. R. B., Lauridsen, E. L. & Jakobsen, M. R. The balance of STING signaling orchestrates immunity in cancer. *Nat. Immunol.* **25**, 1144-1157, doi:10.1038/s41590-024-01872-3 (2024).

53 Woo, S.-R. *et al.* STING-Dependent Cytosolic DNA Sensing Mediates Innate Immune Recognition of Immunogenic Tumors. *Immunity* **41**, 830-842, doi:10.1016/j.immuni.2014.10.017 (2014).

Figures and Figure Legends

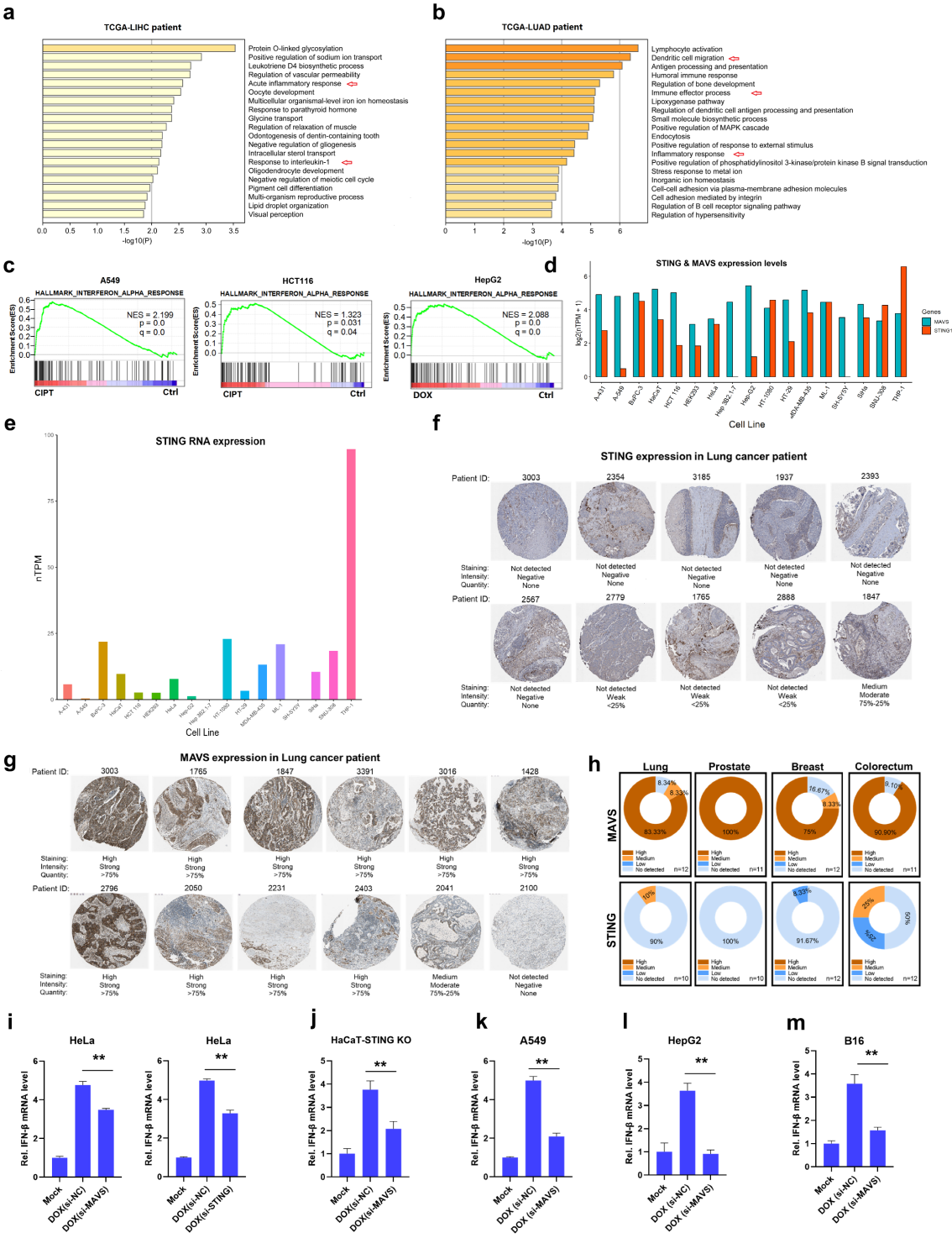

Fig. 1. The Mavs pathway efficiently and broadly mediates chemotherapy-dependent immune responses.

(a, b) GO enrichment analysis of up-regulated gene expression in cancer patients after chemotherapy was conducted based on the TCGA dataset.

(c) Positive correlation between drug treatment and interferon alpha response pathway in the expression profiles from GSE222187, GSE108214, and GSE81878, Nominal P values and FDR q values are shown.

(d) The bar chart shows the expression levels of MAVS and STING across different cell lines, with data sourced from the HPA database.

(e) The bar chart shows the expression levels of STING across different cell lines, with data sourced from the HPA database.

(f) Images showing IHC of STING from the Lung cancer patients in the HPA database.

(g) Images showing IHC of MAVS from the Lung cancer patients in the HPA database.

(h) Pie chart showing the IHC score of STING and MAVS in different patients from the HPA database, where "Not detected" or "Low" indicates low expression, and "High" or "Medium" indicates high expression level of STING and MAVS.

(i) HeLa were transfected with small interfering RNA target STING, MAVS or negative control (NC) for 24 hours and then treated with DOX, IFN-β mRNA levels were measured by RT-PCR.

(j) STING ko HaCaT cell were transfected with siMAVS or siNC for 24 hours and then treated with DOX, IFN-β mRNA levels were measured by RT-PCR.

(k–m) A549, HepG2 and B16 cell were transfected with siMAVS or siNC for 24 hours and then treated with DOX, IFN-β mRNA levels were measured by RT-PCR.

Error bars are mean ± s.e.m. and are representative of 3 independent experiments. Statistical analyses were performed using a one-way ANOVA test with multiple comparisons; $*P < 0.05$.

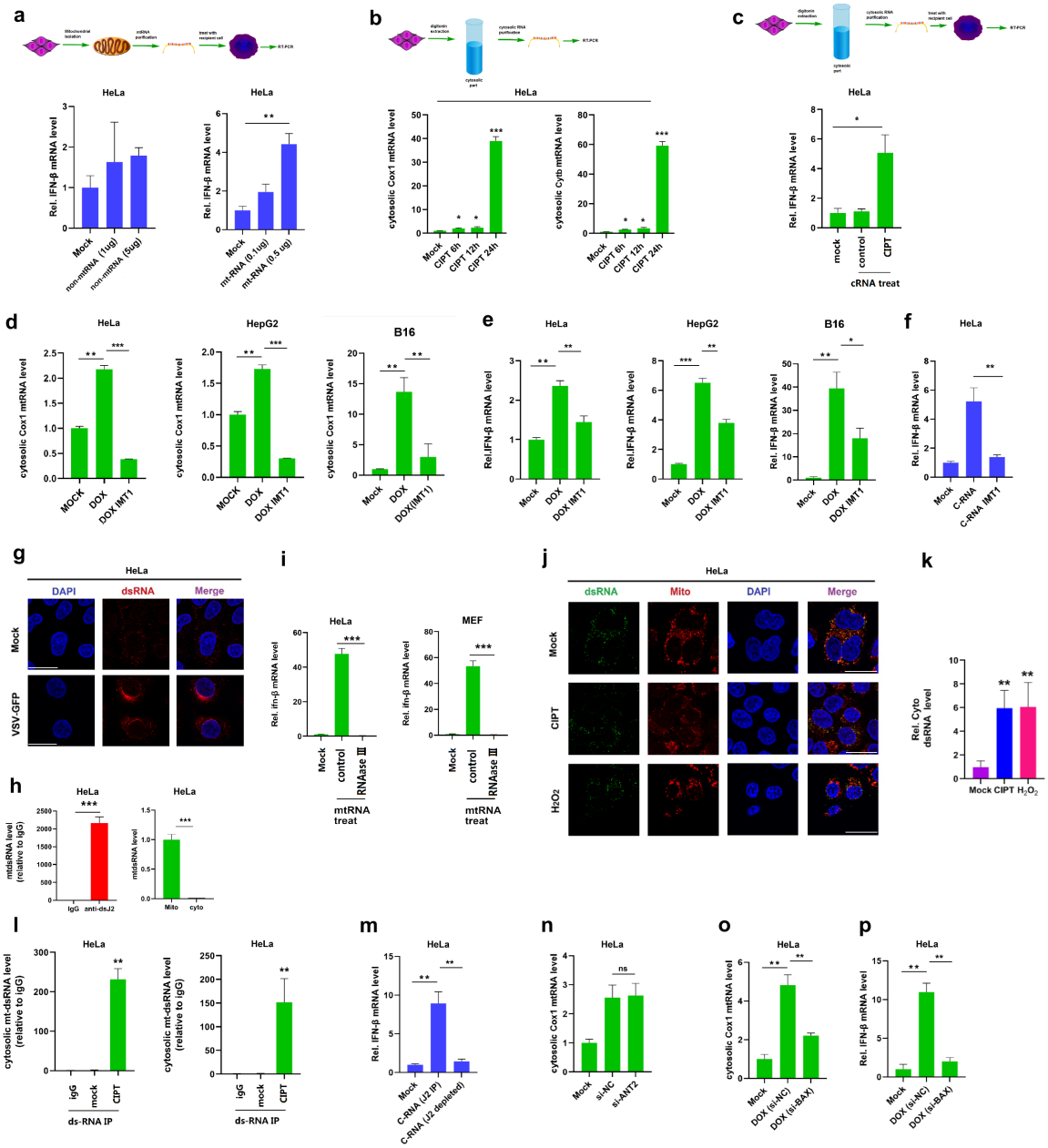

Fig. 2. Mitochondrial double-stranded RNA release triggers MAVS-dependent immune response.

(a) Top: A schematic diagram illustrating mtRNA and non-mtRNA purification and transfection; Bottom: mtRNA and non-mtRNA isolated from donor cells were transfected into recipient cells, and IFN-β mRNA levels were measured by RT-PCR.

(b) Top: A schematic diagram for cytosolic mtRNA (CRNA) purification and analysis; Bottom: cRNAs were extracted from CIPT-treated HeLa, and mtRNA levels were measured by RT-PCR.

(c) Top: A schematic of cRNA purification and transfection; Bottom: cRNAs prepared from

CIPT-treated HeLa were transfected into recipient HeLa, and IFN-β mRNA levels were measured by RT-PCR.

(d) Cell treated with DOX plus IMT1, cytosolic mtRNA level were measured by RT-PCR.

(e) Cell treated with DOX plus IMT1, and IFN-β mRNA levels were measured by RT-PCR.

(f) cRNAs were extracted from CIPT-treated HeLa(C-RNA) or CIPT plus IMT1(C-RNA IMT1), then transfected into recipient cells, and IFN-β mRNA levels in recipient cell were measured by RT-PCR.

(g) Cellular dsRNAs in normal HeLa cells and cell infected with VSV-GFP were detected under immunofluorescence microscope. Scale bar = 20 μ m.

(h) dsRNAs in mitochondrial and cytosolic fractions were immunoprecipitated by dsRNA antibody J2, and detection by RT-PCR.

(i) mtRNAs prepared from donor cells treated with RNase III were transfected into recipient cells, and IFN-β levels were measured by RT-PCR.

(**j, k**) Intracellular localizations of dsRNAs in HeLa cells treated with CIPT or H_2O_2 were examined under an immunofluorescence microscope(**j**), Statistical analysis was performed(**k**). Scale bar = 20 μm.

(**l**) HeLa cells were treated with CIPT. Cytosolic mt- dsRNAs were immunoprecipitated with dsRNA antibody J2 and detection by RT-PCR.

(**m**) HeLa cells were treated with CIPT. Cytosolic mt- dsRNAs were immunoprecipitated with dsRNA antibody J2, then J2-IP dsRNA and J2 depleted RNA purification and transfection into recipient cells, IFN-β mRNA levels in recipient cell were measured by RT-PCR.

(**n**)HeLa cells were transfected with siANT2 or siNC for 24 hours and then treated with DOX, cytosolic mtRNA level were measured by RT-PCR.

906 (**o, p**) HeLa cells were transfected with siBAX or siNC for 24 hours and then treated with
907 DOX, cytosolic mtRNA level were measured by RT-PCR(**o**). and IFN-β mRNA levels were
908 measured by RT-PCR(**p**).
909 Error bars are mean ± s.e.m. and are representative of 3 independent experiments. Statistical
910 analyses were performed using Student's t-test or one-way ANOVA test with multiple
911 comparisons; $*P < 0.05$.
912

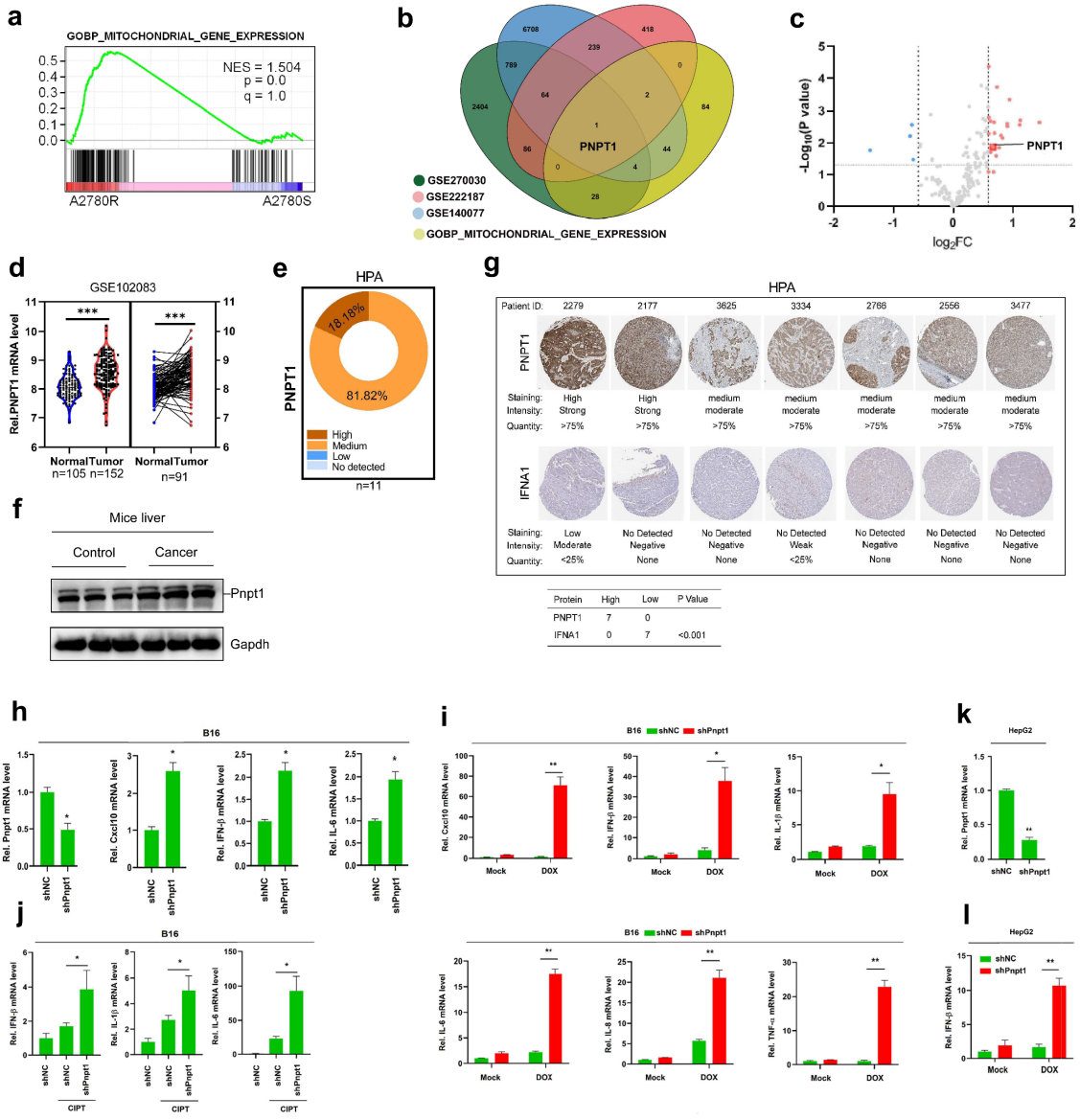

Fig. 3. PNPT1 suppresses mitochondrial dsRNA formation, release, and immune surveillance

(a) GSEA plot of mitochondrial gene expression in the cisplatin resistance group of GSE270030, with NES, nominal p-value, and FDR q-value displayed.

(b) Venn diagram showing that PNPT1 exists in both upregulated genes in GEO datasets (GSE270030, GSE222187, GSE140077) and the mitochondrial gene expression pathway.

(c) Volcano plot illustrating the expression of differentially expressed genes (DEGs) between cisplatin-resistant and sensitive groups (GSE270030).

(d) Unpaired and paired analysis of PNPT1 expression in adjacent normal tissues versus tumor

923 tissues from GSE10283.

924 **(e)** Pie chart showing the IHC score of PNPT1 in hepatocellular carcinoma (HCC) from the
925 HPA database, where “Not detected” or “Low” indicates low expression, and “High”
926 or “Medium” indicates high expression level of PNPT1; antibody HPA034603 was used for
927 PNPT1 detection.

928 **(f)** C57BL/6 mice underwent hydrodynamic injection of transposon-based vectors expressing
929 myr-AKT and NRASV12. When liver cancer formed (after 6 weeks), PNPT1 protein levels in
930 tumor tissue and normal liver were assessed by Western blotting.

931 **(g)** Images showing IHC of PNPT1 and IFNA1 from the same patients in the HPA database,
932 indicating a negative correlation between PNPT1 and IFNA1; correlation analysis was
933 performed using the chi-squared test, where “Not detected” or “Low” signifies low
934 expression and “High” or “Medium” signifies high expression level of PNPT1.

935 **(h)** B16 cells were treated with LV-shNC (shNC) or LV-shPnpt1 (shPnpt1), and mRNA levels
936 of Pnpt1, CXCL10, IFN-β, and IL-6 in B16 cells were measured by RT-PCR.

937 **(i, j)** mRNAs in B16 shNC or shPnpt1 cells were measured by RT-PCR after treatment with
938 DOX and CIPT.

939 **(k, l)** HepG2 cells harboring LV-shNC or LV-shPnpt1 were treated with DOX, and IFN-β
940 mRNA in the treated cells was determined by RT-PCR.

941 Error bars are mean ± s.e.m. and are representative of 3 independent experiments. Statistical
942 analyses were performed using the Mann-Whitney U test, Wilcoxon matched-pairs signed
943 rank test, Student’s t-test, or one-way ANOVA test with multiple comparisons; $*P < 0.05$.

944

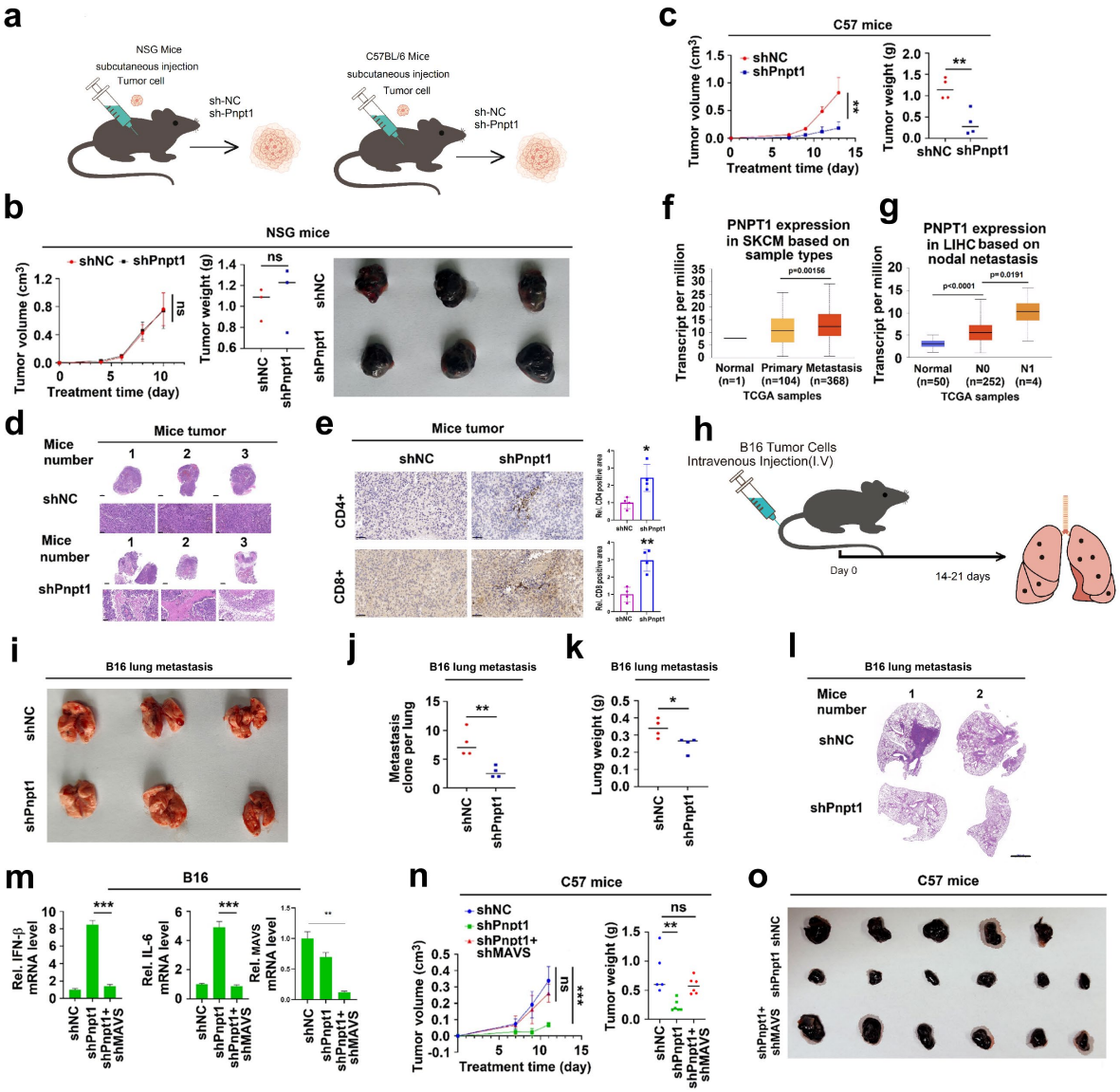

945

946 **Fig. 4. PNPT1 suppresses antitumor immunity in solid tumors**

947 **(a)** Experimental scheme for the subcutaneous tumor model in mice.

948 **(b)** Immunodeficient (NSG) mice were inoculated with shNC-infected B16 cells and

949 shPnpt1-infected B16 cells (n = 3), with tumor growth curves, weights, and sizes determined.

950 **(c–e)** Immunocompetent (C57BL/6) mice were inoculated with shNC-infected B16 cells and

951 shPnpt1-infected B16 cells (n = 4), with tumor growth curves (**c**, left), tumor weights (**c**,

952 right), H&E analyses of tumor tissues (**d**), scale bar = 1000 μm or 100 μm, and CD4+ (**e**, top)

953 and CD8+ T cell (**e**, bottom), scale bar = 50 μm, infiltrations measured.

(f, g) Analysis of Pnpt1 expression in non-metastatic and metastatic tissues from SKCM (**f**) and LIHC (**g**) using the UALCAN portal analysis.

(h–l) Experimental scheme for the B16 lung metastatic tumor model (**h**). Representative images and quantification of lung metastases in C57BL/6 mice inoculated intravenously with shNC-B16 cells or shPnpt1-B16 cells were shown, including metastatic lung (**i**), metastatic clones in the lung (**j**), lung weights (**k**), and analyses of metastatic lung tissues (**l**), scale bar = 2000 μm.

(m) B16 cells infected with shPnpt1 were subsequently infected with shMAVS, measuring IFN-β, IL-6, and MAVS mRNAs by RT-PCR.

(n, o) C57BL/6 mice were inoculated intravenously with shNC-B16 cells (n = 5), shPnpt1-B16 cells (n = 6), and shPnpt1 plus shMAVS-B16 cells (n = 6), with tumor growth curves (**n**, left), tumor weights (**n**, right), and tumor sizes (**o**) determined.

Error bars are mean ± s.e.m. and are representative of 3 independent experiments. Statistical analyses were performed using Student's t-test or one-way ANOVA test with multiple comparisons; $*P < 0.05$.

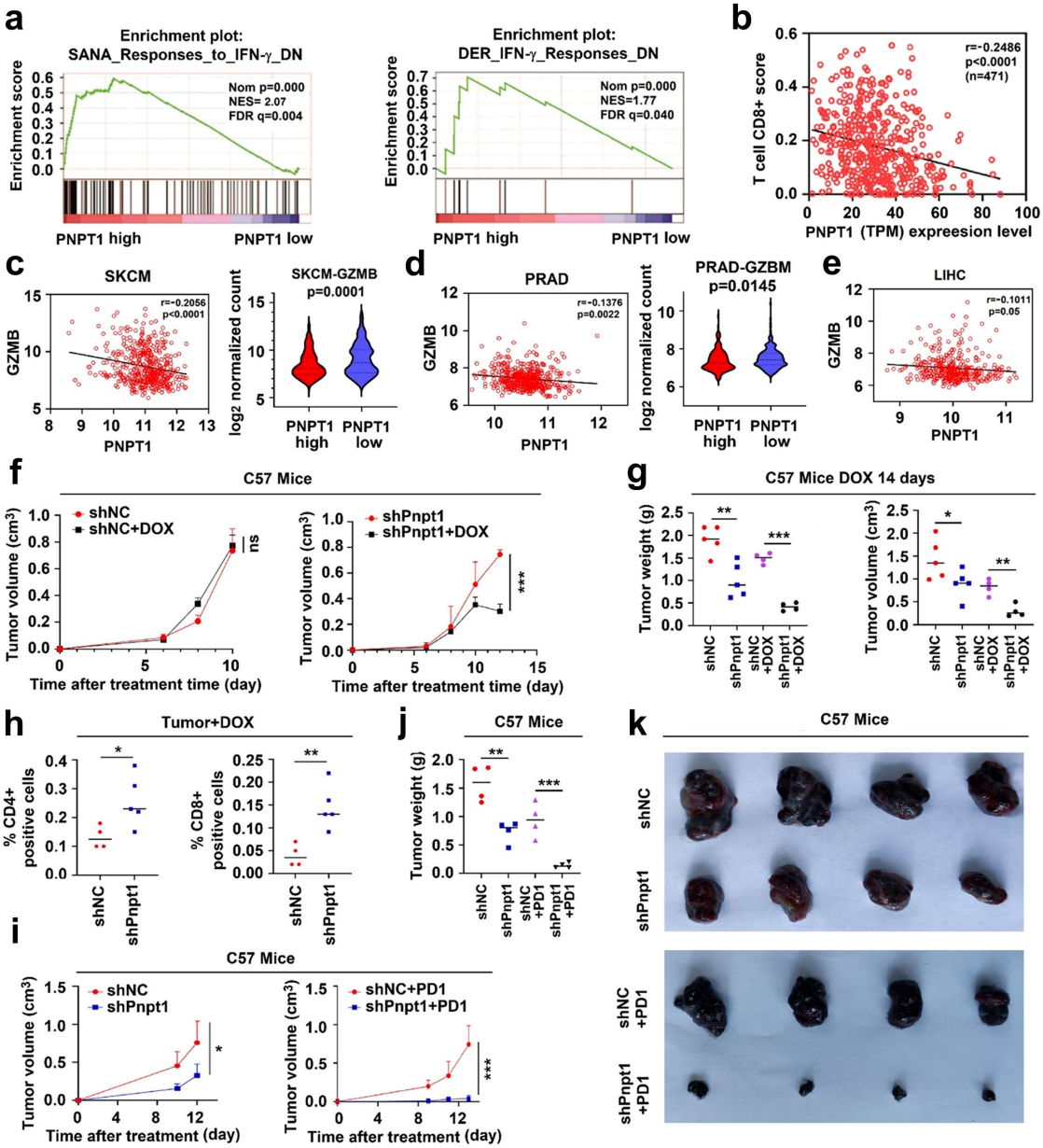

Fig. 5. Loss of PNPT1 overcomes therapeutic resistance

(a) Positive correlation between PNPT1 and IFNγ down pathway in the expression profiles of the TCGA SKCM dataset according to PNPT1 expression level.

(b) Correlation between CD8+ T cells and PNPT1 levels in SKCM patients in the TCGA dataset.

976 **(c–e)** Comparison of GzmB expression between PNPT1 low and high groups in SKCM (C),
977 PRAD (D), and LIHC (E) based on TCGA datasets.
978 **(f)** C57BL/6 mice were inoculated with shNC-B16 or shPNPT1-B16 cells (n = 3) and treated
979 with DOX; tumor growth curves were measured.
980 **(g)** Mice inoculated with shNC-B16, shPNPT1-B16 (n = 5), shNC-B16 with DOX (n = 4), or
981 shPNPT1-B16 with DOX (n = 4), tumor weights and sizes assessed after 14 days.
982 **(h)** C57BL/6 mice were inoculated with shNC-B16 cells treated with DOX (n = 4) or
983 shPNPT1-B16 cells treated with DOX (n = 5). Infiltration levels of $CD4^+$T and $CD8^+$T cells
984 were determined.
985 **(i–k)** C57BL/6 mice inoculated with shNC-B16 (n = 4), shPNPT1-B16 (n = 4), shNC-B16
986 treated with PD1 (n = 4), or shPNPT1-B16 treated with PD1 (n = 4), tumor growth curves (**i**),
987 tumor weights (**j**), and tumor sizes (**k**) determined.
988 Statistical analyses were performed using the Mann-Whitney U test, Student's t-test, two-way
989 ANOVA test with multiple comparisons, or one-way ANOVA test with multiple comparisons;
990 $*P < 0.05$.
991

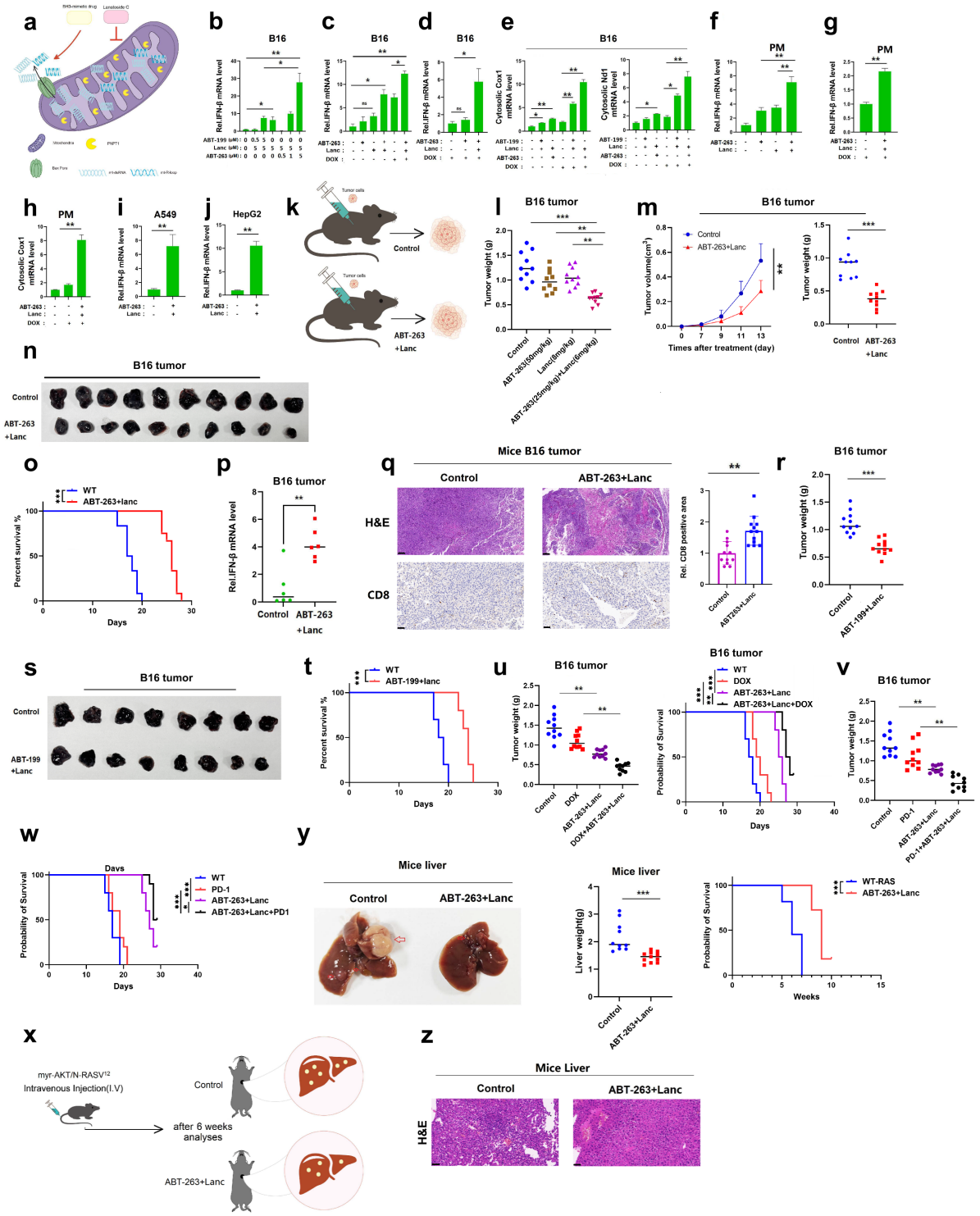

992

993 **Fig. 6. Pharmacological inhibition of PNPT1 synergizes with the BH3 mimetic drugs**

994 **results in robust antitumor immunity and overcomes therapeutic resistance**

995 **(a)** Demonstration of pharmacological inhibition of PNPT1 synergizing with BH3-mimetic

996 drugs.

(b–d) B16 cells treated with various drug combinations for 12 hours and their IFN-β levels measured by RT-PCR.

(e) After 12 hours of treatment with different drug combinations, cytosolic mtRNAs in B16 cells were measured by RT-PCR.

(f, g) PM cells treated with various drug combinations for 12 hours and their IFN-β levels assessed by RT-PCR.

(h) PM cells are treated with different combinations of drugs, after 12h, cytosolic mtRNAs were measured by RT-PCR.

(i, j) A549 and HepG2 cell treated with ABT-263 plus Lanc, after 12h, the IFN-β in the treated cells were measured by RT-PCR.

(k) Experimental scheme of mice B16 subcutaneous tumor model with drug combination treatment.

(l) C57BL/6 mice inoculated with B16 cells and treated with various drug combinations (n = 10 per group) and their tumor weights were determined after 14 days.

(m–o) C57BL/6 mice were inoculated with B16 cells, treated with ABT-263 plus Lanc (n = 10-12 per group) in day 7, 9, and 11. The tumor growth curves; tumor weight (**m**), tumor sizes (**n**) and survival curve (**o**) were determined.

(p, q) C57BL/6 mice were inoculated with B16 cells, treated with ABT-263 plus Lanc (n = 10-12 per group) in day 7, 9, and 11. The IFN-β in the tumor tissues were measured by RT-PCR (**p**). H&E analyses of tumor tissues and CD8+ T cell (**q**) infiltrations measured. Scale bar = 50 μm.

(r–t) C57BL/6 mice were inoculated with B16 cells, treated with ABT-199 plus Lanc (n = 8-12 per group) in day 7, 9, and 11. The tumor weight (**r**), tumor sizes (**s**) and survival curve were determined.

(u–w) C57BL/6 mice were inoculated with B16 cells, treated with different combinations of drugs (n=10-12 per group) in day 7, 9, and 11. The tumor weight and survival curve were determined.

(x) Experimental scheme for hydrodynamic injection of transposon-based vectors expressing myr-AKT and NRASV12 in mice treated with ABT-263 plus Lanc.

(y, z) C57BL/6 mice underwent hydrodynamic injection of transposon-based vectors expressing myr-AKT and NRASV12 (n = 10-12 per group), with liver tumor presentation, liver weight, and survival curve measurements (**y**). H&E analyses of liver tissues(**z**). Scale bar = 50 μm.

Error bars are mean ± s.e.m. and are representative of 3 independent experiments. Statistical analyses were performed using Student's t-test, one-way ANOVA test with multiple comparisons, or two-way ANOVA test with multiple comparisons; $*P < 0.05$.

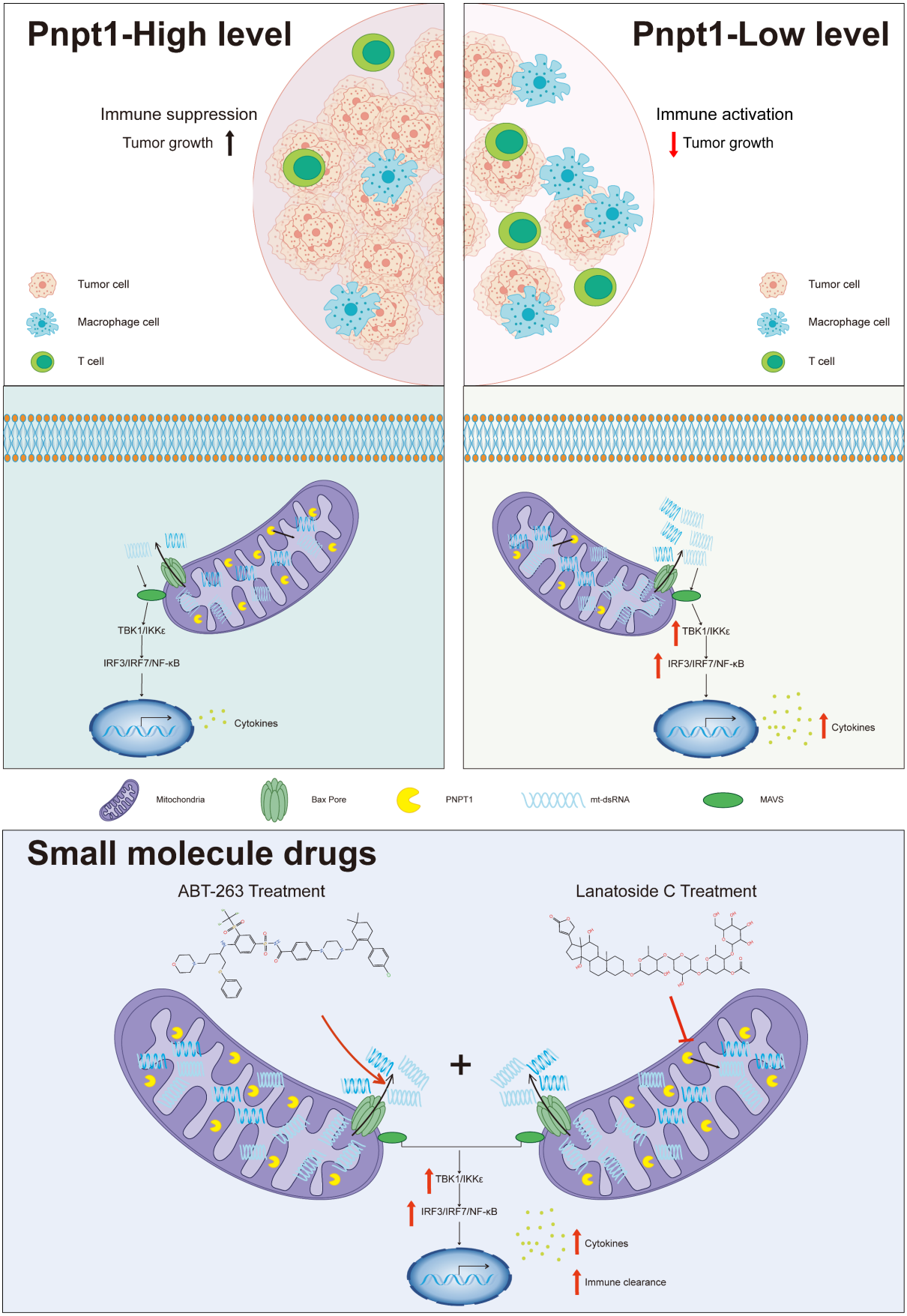

1034

Mechanism underlying PNPT1-mtRNA aix in immune surveillance and anticancer therapy.

On the one hand, upon chemotherapy, mt−dsRNA is released to the cytoplasm via the BAX pore to induce innate immunity and immune surveillance through the MAVS pathway. On the other hand, tumor tissue upregulates PNPT1 to eliminate immunogenic mitochondrial nucleic acids, suppressing immune activation, leading to immune evasion and therapeutic resistance. Finally, pharmacological inhibition of PNPT1 synergizes with BH3-mimetic drugs to efficiently activate mtRNA-mediated antitumor immunity and overcome therapeutic resistance. Our findings suggest that inducing mitochondrial danger signals in combination with PNPT1 inhibition holds promise as an innovative strategy for anticancer therapy.